Stefanie Monika Müller, BSc.

Characterization and Patterning of Lignin Based Thin Films

MASTERARBEIT

zur Erlangung des akademischen Grades

Master of Science

Masterstudium Chemie

eingereicht an der

Technischen Universität Graz

Betreuer

Ass.Prof. Mag.rer.nat. Dr.rer.nat. Stefan Spirk

nstitut für Papier-, Zellstoff- und Fasertechnik, Technische Universität Graz

Graz, Oktober 2018

Stefanie Monika Müller, BSc.

Characterization and Patterning of Lignin Based Thin Films

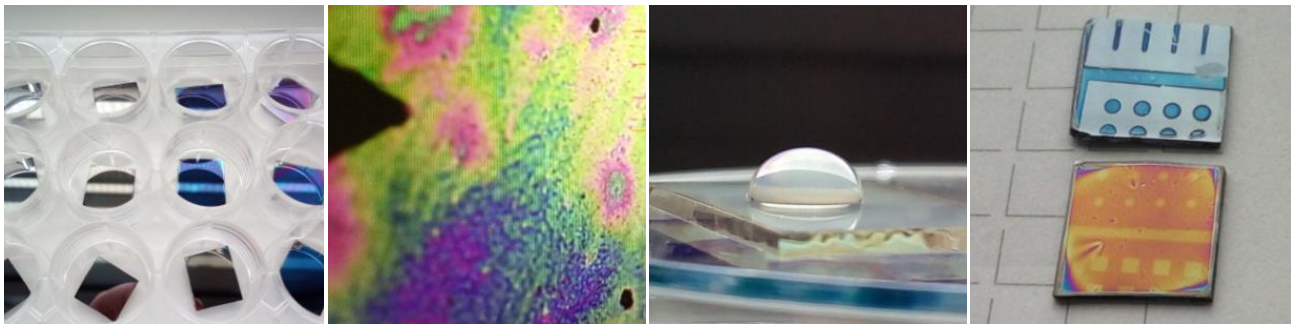

MASTERARBEIT

zur Erlangung des akademischen Grades
Master of Science
Masterstudium Chemie

Eingereicht an der
Technischen Universität Graz

Betreuer
Ass.Prof. Mag.rer.nat. Dr.rer.nat. Stefan Spirk
Institut für Papier-, Zellstoff- und Fasertechnik, Technische Universität Graz

Graz, Oktober 2018

EIDESSTATTLICHE ERKLÄRUNG

Ich erkläre an Eides statt, dass ich die vorliegende Arbeit selbstständig verfasst, andere als die angegebenen Quellen/Hilfsmittel nicht benutzt, und die den benutzten Quellen wörtlich und inhaltlich entnommenen Stellen als solche kenntlich gemacht habe. Das in TUGRAZonline hochgeladene Textdokument ist mit der vorliegenden Masterarbeit identisch.

I declare that I have authored this thesis independently, that I have not used other than the declared sources/resources, and that I have explicitly marked all the material which has been quoted either literally or by content from the used sources. The text document uploaded to TUGRAZonline is identical to the present master's thesis.

10.10.2018

Datum

Unterschrift

ACKNOWLEDGEMENTS

Finding a research topic for my master's thesis that would not only match my interest in renewable resources, but also challenge me in a number of different fields and methods was a long journey. In investigating lignin and its possible use in thin film photo resists I found a suitable, diverse project.

I am grateful to Stefan Spirk for making me part of his research group, for the competent supervision and his helpful advice. For the constant encouragement during the ups and downs of my work, for the opportunity to present a part of this thesis on my first conference and also for giving me a lot of freedom and the space to independently work out solutions, I would like to give special thanks to Stefan Spirk.

The work presented in this thesis would not have been possible without the help from various people, who I want to thank in the following.

First and foremost I have to thank Werner Schlemmer for his constant support from the first minute on and for providing answers to almost all of my questions. Further I want to acknowledge the help from Petra Kaschowitz (NMR) and Josephine Hobisch (GPC) in characterization of the samples, Robin Hofmann and Inge Mühlbacher with contact angle measurements and Max Schmallegger and Thomas Rath in providing the lamps for the UV-illumination experiments. My special thanks go to Krisztina Zajki-Zechmeister for the many hours she invested in this project during AFM measurements.

In addition I want to acknowledge the collegiality, helpfulness and friendly working atmosphere of both, the Institute of Paper, Pulp and Fibre technology and the Institute for Chemistry and Technology of Materials. Special thanks also to my whole research group for making these eight months a time of joy and laughter despite the hard work.

Last but not least, my highest gratitude goes to my family and friends, for supporting me in all situations, encouraging me to go my own way, for giving me fresh motivation, cheering me up and providing the best working environment one can wish for.

ABSTRACT

Lignin is a highly branched phenolic polymer and one of the main constituents of wood. Millions of tons of lignin arise as by-product in paper industry, but only a very small fraction is isolated and used in value-added applications.

In this thesis lignin based thin films were explored to serve as photoactive layers. Such layers are frequently employed in photoresists, materials that change their solubility upon illumination. The first part of the thesis comprises the characterization of the lignins (from Sigma Aldrich and Zellstoff Pöls AG) in terms of gel permeation chromatography (molecular weight), nuclear magnetic resonance spectroscopy (functional groups and degree of substitution) and attenuated total reflection infrared spectroscopy (functional groups). Additionally lignin derivatives (trimethylsilylated and acetylated lignin) were prepared by reaction of the lignins with hexamethyldisilazane and acetic anhydride, respectively, and thoroughly characterized by NMR and ATR-IR spectroscopy.

The second part of the thesis was related to manufacturing of lignin based thin films with tunable properties. After thorough characterization of the films (profilometry, atomic force microscopy, wettability…), their response to UV irradiation was studied in the last part of the thesis. The neat lignins and lignin acetates did not feature sufficient photoactivity. The silylated lignins in turn showed convenient photoactivity in the presence of a photo acid generator. These photo acid generators induce a desilylation reaction upon illumination thereby creating a solubility difference. By employing a photo mask upon illumination, and subsequent development with chloroform, lignin based patterns were obtained.

This thesis provids valuable insights in the solid state conversion of lignin thin films and can be considered the first step for introducing lignin into the field of photoresists.

KURZFASSUNG

Lignin ist ein stark verzweigtes, phenolisches Polymer und einer der Hauptbestandteile von Holz. Millionen von Tonnen an Lignin fallen als Nebenprodukt in der Papierindustrie an, wobei nur ein Bruchteil dessen isoliert und in wertschöpfenden Prozessen verwendet wird.

In dieser Arbeit wurden Lignin basierte Dünnschichtfilme untersucht und deren Performance als photoaktive Schicht überprüft. Derartige Schichten werden häufig in Photoresistoren, Materialien, welche ihre Löslichkeit unter UV-Bestrahlung ändern, eingesetzt. Der erste Teil dieser Arbeit beschäftigt sich mit der Charakterisierung der Ligninen (von Sigma Aldrich und Zellstoff Pöls AG) unter der Verwendung von Gel Permeations Chromatographie (Molargewicht), Kernspinresonanzspektroskopie (funtionelle Gruppen und Substitutionsgrad) und Abgeschwächter Totalreflexions Infrarot Spektroskopie (funktionelle Gruppen). Zudem wurden Ligninderivate (trimethylsilyliertes und acetyliertes Lignin) durch Umsatz mit Hexamethyldisilazane beziehungsweise Acetanhydrid hergestellt und ebenfalls mittels NMR und ATR-IR Spektroskopie gründlich charakterisiert.

Der zweite Teil der Arbeit bezieht sich auf die Herstellung von ligninbasierten Dünnschichtfilmen. Nach umfassender Charakterisierung mittels Profilometrie, Raster Kraft Mikroskopie und Kontaktwinkelbestimmung wurde die Reaktion der Filme auf UV-Bestrahlung untersucht. Die reinen Lignin- und Ligninacetatfilme wiesen nicht genügend Photoaktivität auf. Die silylierten Ligninfilme hingegen zeigten eine ausreichende Photoaktivität unter Anwesenheit eines Photosäuregenerators, welcher unter Bestrahlung eine Desylilierungsreaktion induziert und so einen Löslichkeitsunterschied hervorrufen kann. Unter Verwendung einer Photomaske während der Belichtung und nachfolgender Entwicklung mittels Chloroform wurden ligninbasierte Muster erhalten.

Diese Arbeit bietet Einblicke in die Festkörperumwandlung von Lignindünnschichtfilmen und bildet den ersten Schritt für die Einführung von Lignin in Bereich der Photolithographie.

TABLE OF CONTENT

1. Introduction

1.1. Lignin

Lignin – from the Latin word “lignum” meaning “wood” – is the second most abundant biopolymer after cellulose. As one of the main components of wood, it is the main renewable source of aromatic units and a versatile material with a rich chemical structure (Figure 1) [1].

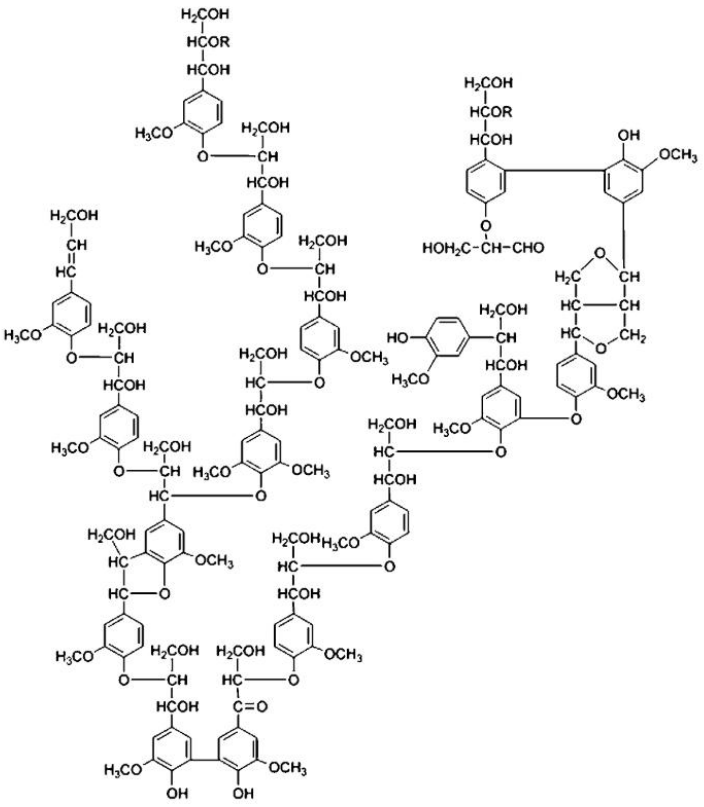

Figure 1: Structural model of lignin by Adler [2].

1.1.1. Structure and Natural Sources

Besides cellulose, hemicelluloses and pectin, lignin is an important component in vascular plants that helps to maintain the integrity of the matrix. It binds individual plant cells as well as carbohydrate polymers together, conferring mechanical strength to the cell wall, protecting plants against microbial attacks and supporting the internal transport of nutrients and water [1,3–5]. Lignin is mainly found in the secondary wall (S1, S2), a part of the cell wall, and the middle lamella (ML), which binds plant cells together (Figure 2). Even though the relative amount of lignin in the ML is higher than in all other parts of the plant, the secondary wall contains the major proportion, due to its higher thickness [1].

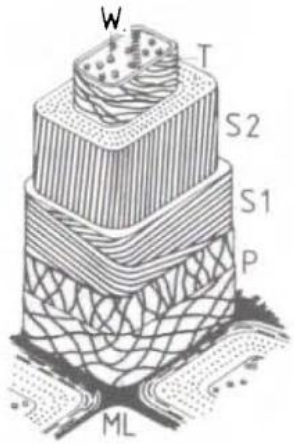

Figure 2: Model of the cell wall structure of wood fibres. ML= middle lamella, P = primary wall, S1 and S2 = secondary wall 1 and 2; T = tertiary wall, W = wart layer [6].

Wood consists of about 15 – 36 % of lignin, strongly depending on the plant species. While hardwoods (e.g. birch) are composed of 40 % cellulose, 35 % hemicelluloses and 20 % lignin, softwoods have a higher lignin content, about 30 % of the total mass [4,7].

Lignin is a complex biopolymer with no defined monomeric repetition unit. It is a physically and chemically heterogeneous material consisting of three main building blocks, called monolignols. A large variety of inter-unit cross linkages lead to different combinations between the building [1,8]. Monolignols are phenylpropane derivatives synthesized from phenylalanine through a multistep process involving various enzymes [7]. The resulting aromatic building blocks of

lignin differ only in the phenyl functionalization, the most abundant being coniferyl alcohol, sinapyl alcohol and p-coumaryl alcohol (Figure 3). Lignin is formed by a random cross-linked polymerization of these phenolic monomers. This process is called lignification and proceeds via a free radical mechanism initiated by cell wall-bound peroxidises or laccases [1,4,7]. The phenolic moieties found in the lignin macromolecules, derived from the monolignols, are then called guaiacyl (G), sinapyl (S) and p-hydroxyphenyl (H) (Figure 3).

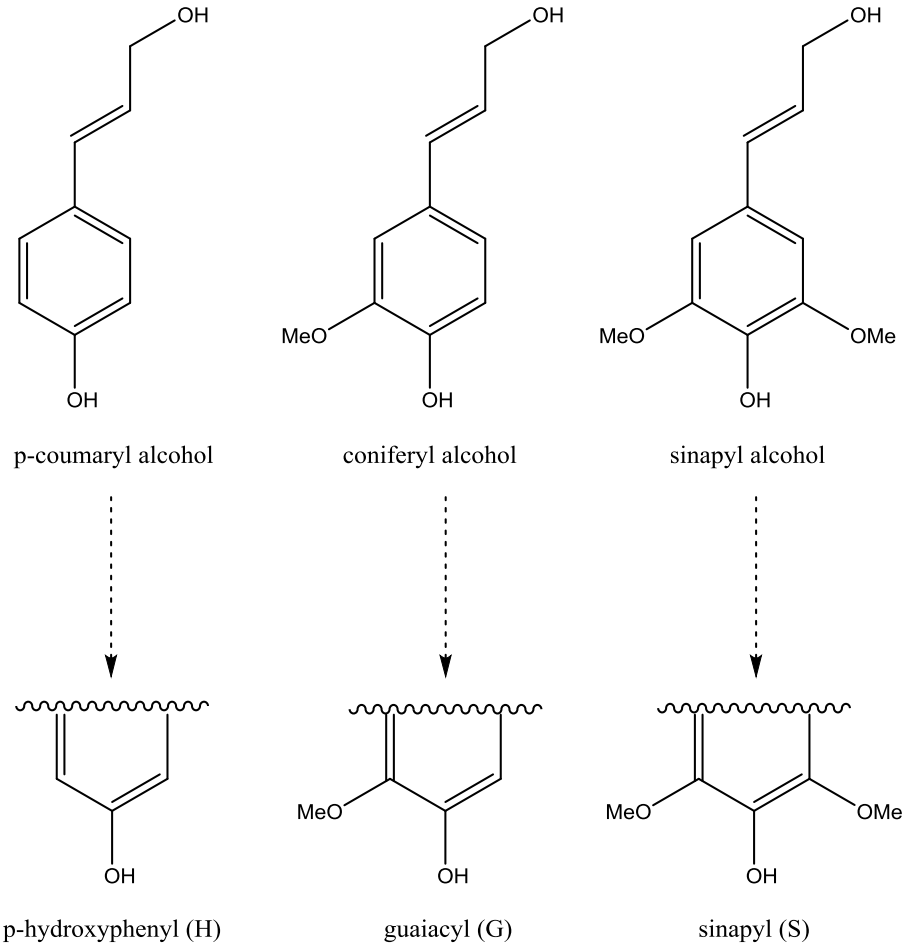

Figure 3: Chemical structure of the most abundant monolignols, coniferyl, sinapyl and p-coumaryl alcohol, and their aromatic residues in the polymer, guaiacyl (G), sinapyl (S) and p-hydroxyphenyl (H) [2,9].

Lignocellulosic material of different botanical origin does not only differ in the proportion of lignin, but also in its composition and cross linking. While hardwood lignins are mainly built from sinapyl and coniferyl alcohols, lignin from softwood mainly contains guaiacyl moieties and herbaceous plants and grasses contain all three basic units (type-H-G-S) [1,10]. In addition to these main

constituents some other phenylpropane derivatives (e.g. arylglycerols, secoisolariciresinol, coniferyl acetate or ferulic acid [1]) are present, but at much lower quantity.

Due to its diverse composition and functional groups, various linkages can be formed in lignin, contributing to the complexity of this biomacromolecule. Monolignols can form C-C and C-O intermonomeric bonds (Figure 4). Aryl ether linkages are the most common linkages with 60 % in hardwoods and 45 - 50 % in softwoods, as the phenoxy radical is stabilized during the radical bond formation [1,11]. Other linkages formed between monomeric units are 5-5′ (biphenyl and dibenzodioxocin), β-5′ (phenylcoumaran), β-1′ (1,2-diaryl propane), α-O-4′ (phenylpropane α-aryl ether), 4-O-5′ (diaryl ether) and β-β′ (β-β-linked structures) [1].

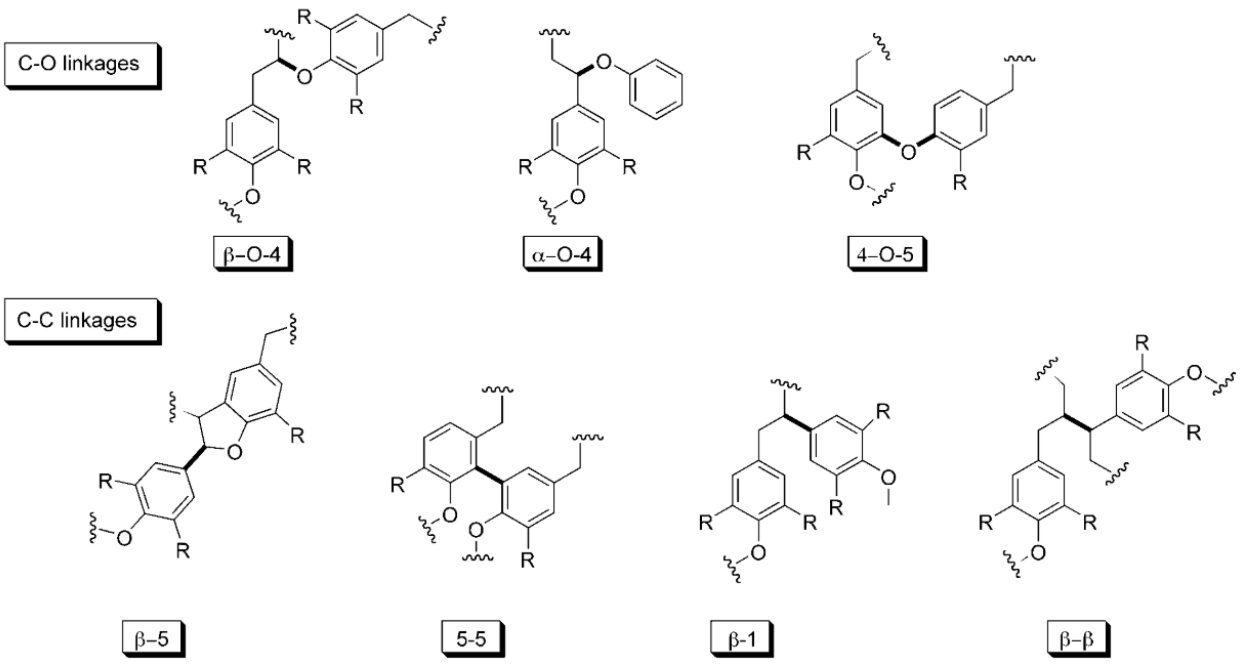

Figure 4: C-C and C-O linkages between monolignols [2].

Lignin, however, does not only intramolecularly form bonds, but also with other cell-wall polymers like polysaccharides and proteins [2]. This leads to the formation of complex three-dimensional networks, the so-called lignin-carbohydrate complex (LCC), with four main types of linkages: benzyl ether, benzyl ester, phenyl glycoside and acetal [1,10]. The occurrence of such stable

intermacromolecular bonds creates significant problems for the structural analysis and isolation of lignin from lignocellulosic material [1,10].

1.1.2. Technical Sources

Lignocellulosic material is the raw material used in the paper industry (Figure 5). In a chemical (or physico-chemical) pulping process, lignin is removed in order to obtain cellulosic fibers. As discussed before (1.1.1), lignin, cellulose and hemicelluloses form a close network (lignin carbohydrate complex; LCC), which makes the separation of these components difficult and requires relatively harsh process conditions [1].

There is a significant number of pulping procedures implemented in industrial scale but just as few different extraction methods, which are used to produce commercially available lignins. There are two types depending on the pulping procedure. The first type are sulfur-containing lignins, which are obtained in the course of the Kraft and sulfite processes, which together account for more than 90 % of the chemical pulp production worldwide [10,12]. The second category are the non-sulfur lignins, like soda lignin, organosolv lignin, steam-explosion lignin and various others [1].

Figure 5: Wood chips before pulping.

Kraft lignin (KL): KL is produced in the sulfate cooking process, where wood is treated with an aqueous solution of Na_2S/NaOH at temperatures of 155-175°C for several hours [2]. The resulting fluid (black liquor) is separated from the solid cellulose, precipitated and neutralized with an acid solution. The dried KL is hydrophobic, water insoluble, but soluble in strong alkali solutions and has a lower molecular mass than the original lignin (1,500-25,000 g/mol [13])[2]. During the process, many reactions take place, resulting in a highly modified lignin regarding its size, condensed structures and substituents. Lignin-carbohydrate

linkages and aryl ether bonds are cleaved, while reactions with hydroxyl and thiol groups take place, introducing new functionalities. The hydroxyl groups present at alkali conditions can cleave α-aryl ether linkages in phenolic units, forming a quinine methide intermediate. In a further reaction hydrosulfide ions can form thiiran intermediates upon elimination of the β-aryloxy group, and eventually a double bond in α-position [14]. In addition, repolymerization occurs via the reaction of internal carbanions with quinine methide (via Michael addition) [1]. Despite the high amounts of pulp produced in the Kraft process, only a minor fraction of lignin is recovered for chemical uses [1].

Lignosulfonates (LS): LS are extracted after sulfite cooking, which is performed at 140-170°C using an aqueous solution of sulfite or bisulfite salts of sodium, ammonium, magnesium or calcium. The variation of the salt sets the pH value for the process, resulting in different reactions and lignin composition [1,15]. In general, lignin is sulfonated, degraded and solubilized during the sulfite cooking [13]. Linkages in the LCC, as well as some β-O-4' bonds are cleaved and phenolic hydroxyl groups and carboxylic groups are formed. In addition, sulfur containing groups are introduced as the aliphatic lignin chain is sulfonated in C_α-position via the intermediate carbocation. The resulting LS are water soluble with both hydrophobic and hydrophilic properties, have a relatively high molecular weight (1000-150,000 g/mol [16]) with a high PDI and contain a high amount of ash [1,13].

Organosolv lignin (OSL): OSL is extracted in the organosolv pulping process by using organic solvents or solvent mixtures. Two of the more common procedures are the Alcell$^{(c)}$ and the Organocell method. Alcell$^{(c)}$ operates at about 180°C using a mixture of water and ethanol, while in the Organocell method the wood chips are pressurized at elevated temperatures (170°C, 13 bar) with methanol, ethanol, alkali and anthraquinone as a catalyst [1]. The resulting OSL are hydrophobic, water in-soluble, sulfur-free and have a high purity. OSL are only marginally modified, however, they also have low molecular masses (500-5,000 g/mol [13]) and only represent the fraction of the lignins in wood, which are soluble in the respective solvent [13].

There are various further processes for wood pulp production and lignin extraction. Some of those lignins are: **Milled wood lignin** (MWL), **cellulolytic**

enzyme lignin (CEL), **soda lignin** (SL), **ionic liquid lignin** (ILL) or **steam-exploded lignin** [1,2,13].

1.1.3. Utilization and Possible Applications

More than 70 million tons of lignin are produced per year worldwide, but only less than 2 % are utilized in value-added applications. The majority is used to generate energy [10,17]. A major part of the electric power of the plant can be obtained thereby, with some plants even exporting electric energy from the surplus obtained [1].

There are numerous potential applications for both, the natural polymer and modified lignin. One of the fields, where lignin is already in use, is quite close to the energy recovery in paper mills. Lignin is added to briquettes or pellets to act as a binder and to improve the fuel properties due to its excellent heating value (26.7 MJ/kg) [1].

The binder properties of lignin, especially lignosulfonates, are used in several applications. Lignin can be added to packing material, reinforcing the packaging and creating a barrier on the sheets. As additive in pelletized animal feed, lignin contributes to a balanced nutrition for the livestock. Further, it is used as a dust repressor on unpaved roads and sport facilities [2,11].

Lignosulfonates are used as emulsion stabilizers in asphalt emulsions, pesticide formulation and dyes, taking advantage of its amphiphilic properties. Lignin can also act as a carrier for ionic nutrients or to remove pollutants such as heavy metals [1].

Due to its highly aromatic character, lignin is known as a free-radical scavenger [8,18]. Antioxidant, antiviral , and even antibiotic and anti carcinogenic activity was reported in various publications [19,20].

Furthermore, lignin can be incorporated into polymers, mostly acting as a phenol substituent, but also as a new, all renewable “bioplastic” (called *Arboform*) [21]. In epoxy resins, lignin can be added as a adjunct cross linking agent in classic epichlorohydrin reactions [2,17].

Lignin nanoparticles can be used as surface treatment in fabrics, utilizing their UV-absorbing properties, or as a biodegradable nanocontainer, by generating hollow capsules [1,22].

For many applications, especially in lignin-epoxy resins, the purity of the lignin is a crucial requirement [17]. Not every lignin sources can be utilized for all applications and varying compositions may lead to altered properties in the materials, which is the main challenge in the incorporation of lignin in any type of material.

Another field of lignin valorization is the production of high-value chemical products. The unique and diverse composition of lignin makes it a promising source for all kinds of aromatic compounds. By depolymerisation, the complex lignin matrix can be broken down to replace chemicals usually obtained from petrochemical industry [1,8]. Vanillin and dimethylsulfoxide (DMSO) are two oxidized lignin products.

Vanillin is produced in a three-step procedure (Figure 6). Sodium vanillate is obtained in an alkaline lignin oxidation step with a copper catalyst [23]. Subsequently, the low molecular compounds are separated via ultrafiltration and are lead through a packed bed with an acid resin for the final conversion to vanillin [2,24,25]. The Norwegian company *Borregaard* is the largest commercial producer of vanillin from lignosulfonate since 1993 [2,24]. However, there is a high pressure on the vanillin price and a constant struggle for economical viability.

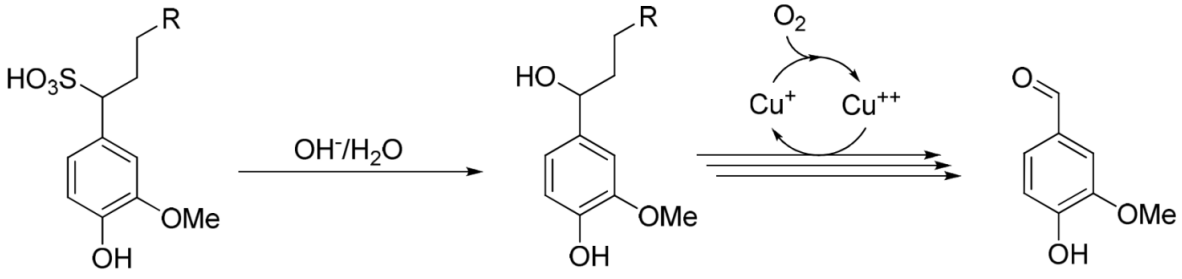

Figure 6: Reaction scheme of the production of vanillin from lignosulfonate.

Another chemical, namely DMSO, can be obtained from kraft pulping. Dimethylsulfide (DMS) is the product of a demethylation reaction of lignin upon treatment with molten sulfur in alkaline media (Figure 7). In the course of this reaction, two methyl groups are transferred to the sulfur atom. The resulting DMS is oxidized and converted to DMSO. This process, based on a renewable raw material, avoids odorous by-products (as in the petrochemical pathway) and processes the waste stream for the recovery of papermaking chemicals [1,2].

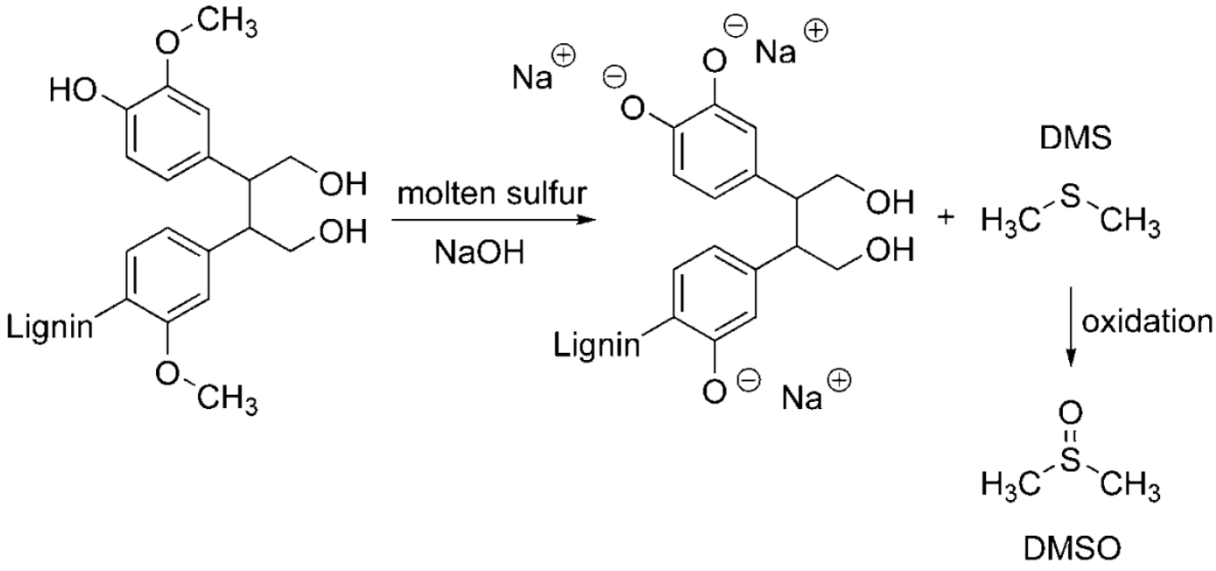

Figure 7: Reaction scheme of the production of DMSO from lignin [2].

By heating lignin to rather high temperatures, it can be utilized as active carbon material or as syngas in gasification processes. Lignin derived syngas shows the advantage of a sulfur-free and metal-free raw material and a reduced need of purification relating thereto [1].

1.2. Lignin Thin Films

Thin films provide a good opportunity to study fundamental properties of lignin in the solid state. The simplified systems help to investigate many physicochemical phenomena and surface interactions [3,22,26]. Since the first preparation of model thin films by Lee and Luner [27], several more advanced film preparation methods were developed.

1.2.1. Coating Methods

All methods of thin film formation involve some kind of solvent evaporation. The most basic and first of all applied methods for preparing a thin film is the solvent evaporation of a drop of material solution on a substrate. Like the first thin films Micic et al. used *a drop of suspension [...] placed on the bottom of a Petri dish and let it dry at room temperature [28]*.

In the Langmuir-Blodgett technique, very thin films are deposited from the water surface by emersing (or immersing) a substrate from the solution. A solution of e.g. polymer or nanoparticle solution is added onto the water surface. Via evaporation (e.g. with chloroform) or mixing (e.g. with methanol/water solution) a layer of pure polymer/nanoparticles is formed (Figure 8). Depending on the volume of molecules added and the available space on the water surface, a monolayer of molecules can be formed. By emersing a hydrophilic substrate from the water and moving the barriers towards the substrate to maintain constant surface pressure, a homogeneous film is deposited on the substrate surface [29].

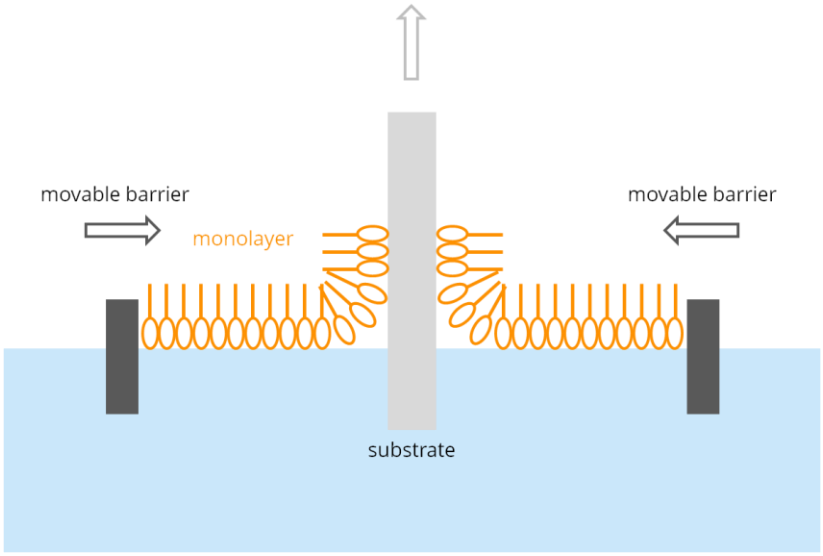

Figure 8: Langmuir-Blodgett technique for thin film formation [30].

Another method for thin film formation is the spin coating technique. After fixing a substrate onto a rotating disk, a material solution is spread on the smooth substrate surface and the substrate is rotated at a certain speed to spread the solution, remove redundant fluid and evaporate the solvent [31]. After the spin

coating cycle all of the solvent should be evaporated and a continuous film is left on the substrate surface (Figure 9). There are many parameters influencing the film properties, most important; the concentration and viscosity of the solution, solvent volatility, spreading and wetting properties, acceleration, rotation speed, spin time and the properties of the polymer itself (complete solubility, dispersion, formation of aggregates) [31,32].

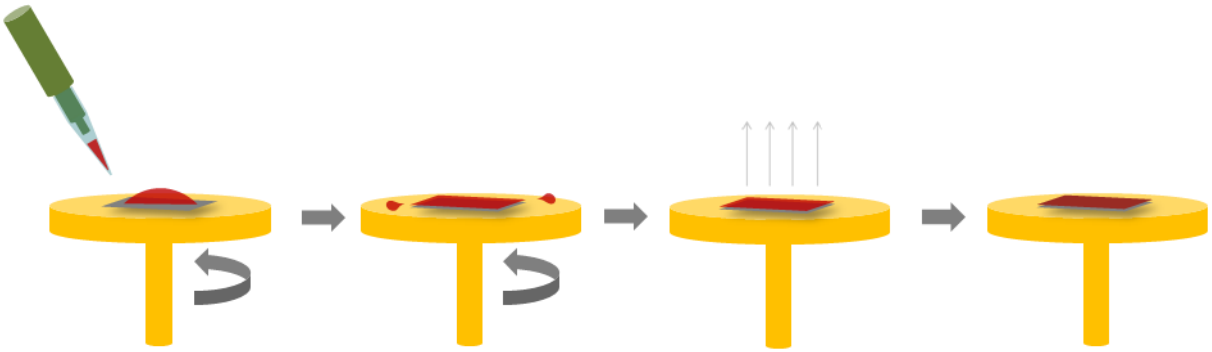

Figure 9: Scheme of the spin coating process.

Spin coating was the technique used in the following work to achieve uniform, continuous thin films of low roughness.

1.2.2. Thin Films From Lignin Solutions

When spin coating unmodified lignin the possibilities are limited to the solubility of the biopolymer. Soda and Kraft lignins are poorly soluble in most organic solvents. To dissolve lignin polar aprotic solvents such as DMSO, DMF or pyridine or basic aqueous conditions are needed [8]. According to Norgren et al. [31] the only solvent where no self-aggregation of the lignin molecules was found, was ammonium hydroxide. NH_4OH has another advantage over alkaline solutions from e.g. sodium hydroxide. Due to its fast decomposition to NH_3 and H_2O at equilibrium, the ammonium ion is readily removed from the solution while spin coating. This leads to a decrease of the pH value at the surface and a resulting decrease in solubility of the lignin (due to ion exchange from NH_4^+ to H^+). Another drawback of using NaOH is the salt excess built up at the surface of the film when the water is evaporated. Sodium ions have to be removed after film formation by rinsing with deionised water, exchanging the Na^+ with H^+ in the lignin molecule [31].

Different lignins can be spin coated from different solvents, according to their solubility. Milled wood lignin, for example, can be spin coated from 1,4-dioxane (0.5 wt%; 0.4 nm thickness; smooth [33,34]) or an acetone:water solution (9:1; 1.0 wt%; 30-60 nm; smooth [3]).

1.2.3. Thin Films From Lignin Derivatives

With the derivatization of lignin the solubility can be altered. The introduction of hydrophobic groups (e.g. acetyl, trimethyl silyl or palmitate) makes lignin available for a broader range of organic solvents like THF or chloroform. The good dissolution behaviour of lignin in these solvents and their volatility improve the formation of a smooth thin film. By dissolving lignin acetate or palmitate in chloroform, a mixture of AcL and cellulose derivatives (TMSC) can be used to create cellulose-lignin blend films [35–37].

1.3. Photolithography

Photolithography is the go-to technique for the formation of three-dimensional reliefs in the production of integrated circuits (ICs) and other microelectronic devices [38]. It is a method to transfer precise patterns from a mask onto a substrate or thin film using light. There are two commonly used types of photolithography depending on the light source; Optical lithography uses light in the visible spectrum, while UV-lithography uses UV-light. Extreme ultraviolet (EUV), advanced e-beam, nanoimprint, scanning probe, and ion beam lithography are some next-generation lithography processes [38,39].

In the photolithography process, there are four main steps (Figure 10): The application of a photo-sensitive layer onto a substrate, the creation of a solubility difference via illumination with a mask, the development of the pattern in the film and the etching of the substrate (or deposition of a new layer) [39]. There are often multiple layers of materials coated onto the substrate for more complicated systems and multiple etching [38].

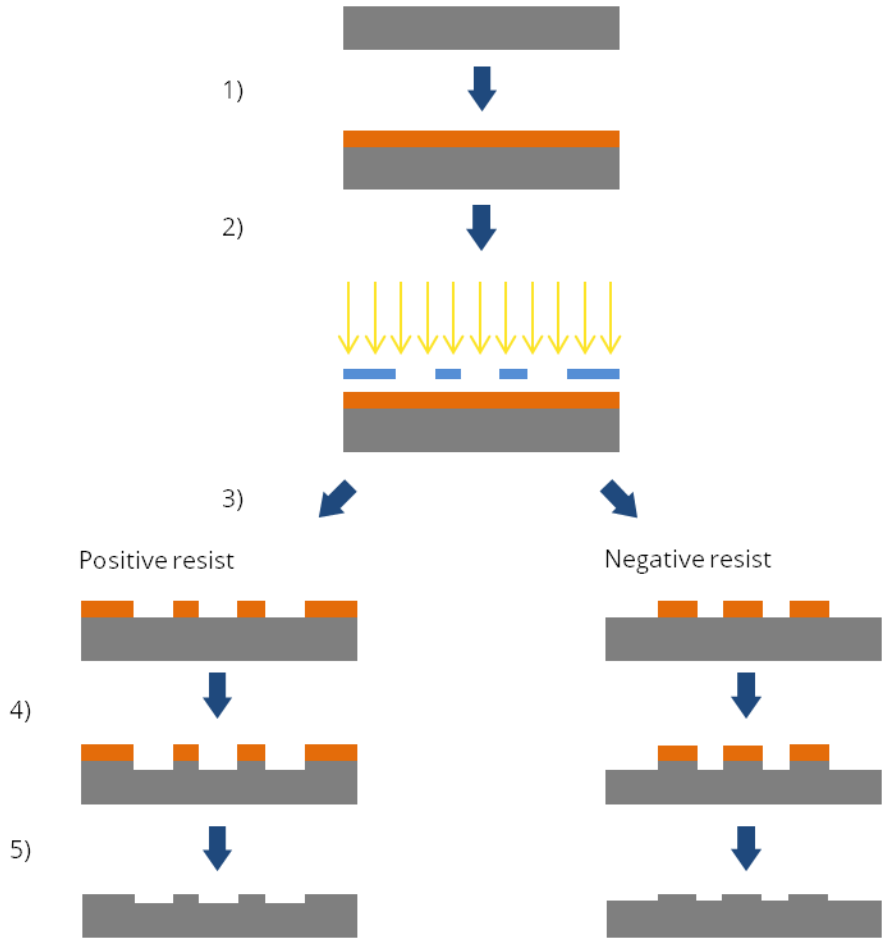

Figure 10: Photolithographic process. 1) coating of the photoresist; 2) illumination with a photo mask and light; 3) development of the pattern by solubility difference; 4) etching of the substrate; 5) removing of the photoresist.

1.3.1. Photoresist

The photo-sensitive material applied on the substrate is called *photoresist*. A photoresist undergoes changes via UV-illumination leading to altered dissolution behaviour in a specific solvent.

There are two types of resists, positive and negative. Positive-tone resists are dissolved where the film was exposed to light, whereas the shaded areas remain solid. Negative-tone resists ensure the removal of the unexposed parts while the illuminated areas remain. The difference in solubility behaviour can occur due to a change in the functional groups, an altered polarity or a cross-linking reaction, for instance [38–40].

1.3.2. Photo acid generator

If light does not naturally change the solubility of a photoresist layer (like lignin), it can be mixed with a photo-active substance, which induces a reaction. One class of compounds comprises *photo acid generator (PAG)*, as it produces protons upon irradiation.

There are different types of PAGs with sulfonic acids, trifluoromethanesulfonic acid (triflic acid) or HCl. When a PAG absorbs a photon it enters an excited state. When returning to the ground state a bond can be cleaved and, over a series of rearrangements, an acid is set free. The produced acid acts mainly as a catalyst, which makes the photoresist with PAG a chemically amplified resist (CAR). CARs can cause multiple reactions by only one single photon uptake, amplifying the impact. This catalytic effect enhances the sensitivity and the overall efficiency of the photolithographic process [41].

An important step in photolithography with CARs is the post exposure bake (PEB) often also referred to as dark reaction. This process step allows for diffusion of the generated acids and smoothing of the spatial distribution of photo acids after illumination. The diffusion length should be large enough to effectively blur out the spatial distribution, but small enough to keep the acids from trespassing the exposed area and to prevent widening of the desired pattern [38,39].

1.4. Surface properties

To study the surface properties of lignin is a demanding task. Lignin is a highly heterogeneous biopolymer, and its composition varies depending on the source (hardwood, softwood, plant species) and the extraction technique (like MWL, SL or KL). Up to now it is not possible to study lignin in its naturally occurring, unaltered form, but only after extraction from wood and some structural alteration related thereto [3]. Nevertheless, there are numerous studies [8,22,35,42] on the surface energy and wettability properties of different lignins, trying to understand fundamental processes in nature (e.g. water and nutrient transport in trees) and the role of lignin thereby [31].

1.4.1. Surface energy and wetting

Wetting is a term describing the interaction of a liquid with a solid, meaning the spreading of a liquid over a surface or the penetration into the material. To determine the wetting ability of a certain liquid on a specific solid surface, contact angle determinations can be performed (Figure 11). A drop is placed on the surface and the wetting ability can be calculated as a function of the surface energy of the solid-gas interface, the liquid-gas interface and the solid-liquid interface (Figure 11) [43]. Contact angles of less than 90° indicate a wetting liquid. An example for this is the combination of water on a hydrophilic material. The water spreads as the adhesive forces (between the water and the solid surface) exceed the cohesive forces of the liquid. The force resulting from intermolecular bonds or cohesive forces between the molecules is called *surface tension*. It "*can be understood from the perspective of the force required to start peeling off a certain width of adhesive tape (Gao 2009)*" [44]. Surface tension is a force, acting perpendicular to a line on the surface with the units N/m. However, it can also be given as J/m^2 and is numerically equal to the *surface energy*, which is given with the same units. *Surface energy* can be described as a measure of the energy required to form the unit area of a new surface interface [45].

The thermodynamic wetting can be described by the Young equation (eq. 1),

$$\sigma_{sg} = \gamma_{sl} + \sigma_{lg} \cdot cos\theta + \pi_e \qquad \text{(eq. 1)}$$

where σ_{sg} ,σ_{lg} and γ_{sl} are the interfacial free energies of solid, gas and liquid phase (Figure 11) and π_e is the equilibrium pressure of adsorbed vapor of the liquid on the solid. π_e is assumed to be 0. The total free energy at the surface can be described as the sum of the contributions of the polar (hydrogen bonding; superscript P) and disperse force (superscript D) at the surface. For the case, that both forces operate, the derived equation for the free energy of the interface between solid and liquid is (eq. 2):

$$\gamma_{sl} = \sigma_{sg} + \sigma_{lg} - 2(\sqrt{\sigma_{sg}^{D}\sigma_{lg}^{D}} + \sqrt{\sigma_{sg}^{P}\sigma_{lg}^{P}}) \qquad \text{(eq. 2)}$$

Values for σ_{lg}^{D} and σ_{lg}^{P} have been published for many liquids. Therefore disperse and polar contributions of the surface tension of the solid can be calculated by measuring the contact angle of two liquids with the same surface and using the following equation (eq. 3):

$$\frac{(1+\cos\theta)\cdot\sigma_{lg}}{2\cdot\sqrt{\sigma_{lg}^{D}}} = \sqrt{\sigma_{sg}^{D}} + \sqrt{\sigma_{sg}^{P}}\cdot\sqrt{\frac{\sigma_{lg}^{P}}{\sigma_{lg}^{D}}} \qquad \text{(eq. 3)}$$

A plot of $\frac{(1+cos\theta)\cdot\sigma_{lg}}{2\cdot\sqrt{\sigma_{lg}^{D}}}$ vs. $\sqrt{\frac{\sigma_{lg}^{P}}{\sigma_{lg}^{D}}}$ gives a straight line and the polar and dispersive component of the surface energy can be derived from the slope and the intercept, respectively [46].

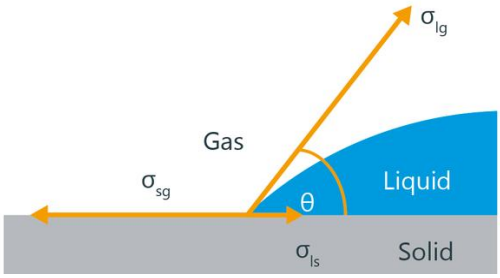

Figure 11: Forces in the contact angle measurements and surface energy calculation [47].

The equations presented above do apply for ideal, perfectly smooth surfaces. In real surfaces the surface roughness can be taken into account by adding a roughness factor, describing the ratio between the actual and projected solid surface area (being >1 for rough surfaces). For the validity of this factor, the

liquid needs to be able to wet the whole surface and penetrate into the grooves. This ability decreases when the droplet is larger than the roughness by a scale of two or three orders of magnitude. In this case the Cassie equation (eq. 4; [48,49])

$$\cos\theta_m = x_1 \cdot \cos\theta_{y1} + x_2 \cdot \cos\theta_{y2} \qquad \text{(eq. 4)}$$

applies and the surface is treated like a heterogeneous surface, with air as the second phase. θ_{y1} and θ_{y2} are the contact angles for the pure component with the contact angle of water with air being 180° and θ_m is the measured contact angle of the aggregate. x_1 and x_2 are the area fractions of the different chemistries [50]. Half a decade later, Gao and McCarthy pointed out, that *"contact angle behavior is determined by interactions of the liquid and the solid at the three-phase contact line alone and that the interfacial area within the contact perimeter is irrelevant (Gao and McCarthy, 2007)"*. Contact angles of surfaces with chemically heterogeneous islands were investigated and it was shown, that they have no influence on the contact angle compared to the homogeneous surface if the island is completely buried under the liquid drops [51,52].

Looking at lignin, the surface energy depends on the composition (origin and isolation method of lignin), but also on the evaluation technique, the surface preparation method and consequently the surface height profile. Notley and Norgren (and in 1972 also Lee and Luner [27]) investigated surface energies of different lignins. They found, that there were no significant wetting differences between lignins of different preparation and the surface energy of MWL and KL is in the range of 53-56 mJ/m^2. However, Kraft lignin shows a significantly higher polar component due to the charged chemical groups introduced during the extraction process [3,22].

Buono et al. looked at the change of hydrophobicity upon introduction of acetyl and silyl groups (Figure 12). They found a rapid increase of the water contact angle and reduced wettability with increasing degree of substitution. It was also shown that the water contact angle of the used soda lignin (SL) was smaller than previously reported for Kraft and milled wood lignins, which can be related to the high amount of phenolic hydroxyl groups in SL. However, it is difficult to compare the sole measurement of the water contact angle, as it mainly accounts for the polar proportion of the surface energy and the calculation of the free

surface energy needs contact angle measurements with at least two liquids with known surface tension.

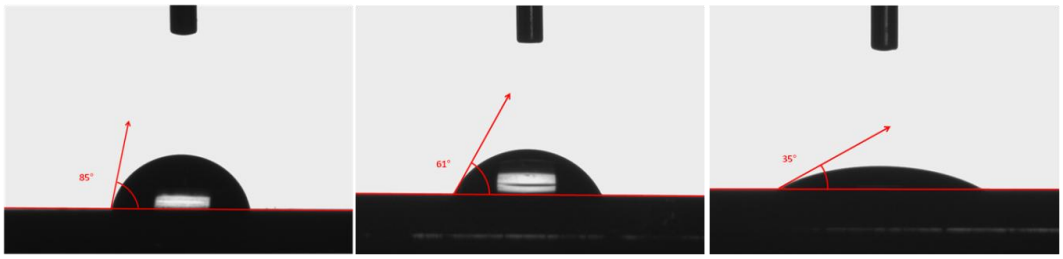

Figure 12: Contact angle determination of water drops on different substrates. (From left to right: silylated, acetylated and regenerated lignin).

1.4.2. Solubility and self assembly

Lignins exhibit different solubility mostly depending on their origin and extraction process, as mentioned before (1.1.2). The alteration of the natural occurring lignin is inevitable in order to separate the polymer from cellulose and hemicelluloses in the wood matrix, thus changing its original properties.

A typical characteristic of polymers is the decreased solubility with increased molecular mass. Lignin follows this trend to a certain extent, but is far more dependent on the amount of groups accessible to solvation than the macromolecular size [53]. Lignin shows intermolecular hydrogen bonding and π-π interactions, complicating the solvation in common solvents.

There is a difference between H-bonding from aliphatic and phenolic hydroxyl groups, with aliphatic OH-groups forming stronger hydrogen bonds than other types. The fewer aliphatic groups there are in the lignin, the easier is the solubilisation[54]. In addition softwood lignin should be more difficult to solubilise than hardwood, due to the elevated content of guaiacyl units, which exhibit stronger π-π interactions [55]. Interaction and association between different structural elements of lignin result in an assembly of organized macromolecular clusters of different densities [54,56]. This self-aggregation takes place in order to minimize the free energy of the system and results in aggregates of well-defined cylindrical building blocks with 4-10 monolignol units. The building blocks can be arranged in larger aggregates, forming random coils, two-dimensional objects, isotropic or network-like structures [9].

2. Starting Point and Motivation

Lignin is the main side (or waste) product in the paper industry. With the combustion of the residual black liquor and the utilization of lignin for energy regeneration a valuable natural material is burnt.

Within the past few years the interest in wood and wood derived polymers (cellulose, lignin and xylans) and their use in new fields beyond traditional applications (i.e. paper, textiles or additives) has grown. Research was guided towards the introduction of renewable materials into conventional processes and products.

One process, where lignocellulosic components could replace well-known materials is micropatterning, or more precisely photolithography. Photolithography is the go-to technique for the formation of three-dimensional reliefs in the production of integrated circuits (ICs) and other microelectronic devices [38]. It is a method to transfer precise patterns from a mask onto a substrate or thin film using light and a photoactive layer, called photoresist. Currently the most common photoresists are epoxy based polymers, like the EPON® resin SU-8 (from Shell Chemical) [57], or novolac resins containing a diazonaphthoquinone as a photoactive compound [58], exhibiting a negative or positive tone resist respectively. By replacing (or only partly replacing) those films made of synthetic polymers with lignin for example, could lead to high value-addition of wood based materials.

2.1. Research Objectives

To introduce lignin to this new field of research, basic properties of lignin in thin films need to be characterized and its suitability as a photoresist needs to be evaluated. For characterization, the tools of choice are atomic force microscopy, profilometry, IR-spectroscopy, NMR-spectroscopy, GPC and contact angle measurements.

After characterization, the main point of interest is to create a pattern in a lignin thin film solely by UV-irradiation.

The objectives of this research are as follows:

- Characterization of different lignin samples, focusing on solubility behaviour and differences between batches.
- Derivatization of lignin to change certain properties and making lignin more available for photo-interactions.
- Formation of tunable thin films of lignin derivatives.
- Observation of the effect of UV-irradiation on lignin and lignin derivative thin films (structural changes and solubility).
- Optimization of the process parameters for patterning.

3. Experimental

3.1. Chemicals

Kraft lignins were obtained from Sigma Aldrich (Lignin, alkali) and Zellstoff Pöls AG in cooperation with Marlene Kienberger (TU Graz). The latter ones were washed with acid, with water or used without washing (Table 1).

Table 1: Desciption of the used lignin samples.

Short name	provided from	treatment	used in experiments	derivative sample names
S1	Sigma Aldrich	untreated	acetylation; silylation	Ac1S1; Ac2S1; Si1S1; Si2S1; Si3S1
S2	Pöls	water washed	acetylation	not used
S3	Pöls	unwashed*	acetylation	Ac1S3; Ac2S3;
S4	Pöls	water washed*	acetylation	Ac1S4
S5	Pöls	acid washed*	acetylation; silylation	Ac1S5; Si1S5

*detailed description in appendix

Acetic anhydride (≥99% from Sigm Cambridge Isotope Laboratories Inc., Cambridge, GB a Aldrich, St. Louis, USA), pyridine (≥99 %, for synthesis; Carl Roth GmbH, Karlsruhe, Germany), hexamethyldisilazane (HMDS; reagent grade; ≥99 %; from Sigma Aldrich, St. Louis, USA) and chlorotrimethylsilane (TMSCl; ≥99.0 % GC; from Fluka, Honeywell international Inc., Morristown, USA) were used for the derivatization reactions. THF (99% from Carl Roth GmbH, Karlsruhe, Germany), DMF (99.5 %; from Carl Roth GmbH, Karlsruhe, Germany), chloroform (99.3 %; stabilized with about 0.6 % ethanol; from VWR Chemicals, Radnor, USA) and ammonium hydroxide (ca. 28 % in water; from Fluka, Honeywell international Inc., Morristown, USA) were utilized as solvents. N-hydroxynaphtalimide triflate (electronic grade ≥99 %; from Sigma Aldrich, St. Louis, USA) and 2-(4-Methoxystyryl)-4,6-bis (trichloromethyl)-1,3,5-triazine (98 %; from Sigma Aldrich, St. Louis, USA) were used as photo acid generators and hydrochloric acid (37 %; VWR Chemicals, Radnor, USA) for vapour regeneration.

For the cleaning of the substrates sulfuric acid (95 %) from VWR Chemicals and hydrogen peroxide (30 %; stabilized) from Carl Roth were used. For the contact angle measurements Milli-Q water from the internal supply and copper stabilized diiodo-methane (99 %; abcr GmbH, Karlsruhe, Deutschland) were used. Pentafluorobenzaldehyde (98% from Alfa Aesar, Haverhill, USA), deuterated chloroform and DMSO-d (both 99.80 % D; Euriso-top, Cambridge Isotope Laboratories Inc., Cambridge, GB), 2-Chloro-4,4,5,5-tetramethyld-dioxaphospholane (95% from Sigma Aldrich), Tris(2,4-pentanedionato) chromium(III) (98% from TCI Chemicals, Tokyo, Japan) and cyclohexanole (99 % from Sigma Aldrich, St. Louis, USA) were purchased for NMR measurements.

3.2. Substrates and Materials

3.2.1. Substrates

Thin films were spincoated on glass, silicon wafers and gold substrates. The glass substrates were cut from standard microscopy slides (from Carl Roth GmbH, soda-lime glass; 76 x 26 mm), the Si-slides were cut from single side polished silicon wafers from Siegert Wafers (Aachen, Germany; 675 ± 25 µm thick) and the gold substrates were reused gold coated glass SPR-slides from BioNavis (Tampere, Finland; D263; 50 nm thick; 1 cm x 2 cm).

3.2.2. Cleaning of the substrates

The substrates were rinsed with deionized water, dried under a stream of nitrogen gas and immersed into “Piranha” acid (peroxymonosulfuric acid). The “Piranha” acid was prepared in-situ by mixing sulfuric acid (95%) and hydrogen peroxide (30%) in a 3:1 v/v ratio. Glass and silicon substrates were cleaned for 20 minutes, while gold substrates were only cleaned for 3 minutes and the “Piranha” acid was allowed to cool down to room temperature beforehand. After the “Piranha” acid bath, the substrates were rinsed with deionized water again and stored in deionized water until used. Before spin coating the substrates were rinsed with deionized water, dried under a stream of nitrogen and again dried by rotating on the spin coater (from Pollos, Putten, Netherlands) for 10 seconds.

3.3. Lignin derivatization

3.3.1. Acetylation of lignin

The acetylation of ligin was performed with 0.5 g of lignin with a known content of hydroxyl groups. In a typical procedure, 2.5 equivalents of acetic acid anhydride (1.15 g, 1.06 ml, 11.24 mmol), with respect to the hydroxyl groups (10 mmol/g lignin) in the dry lignin sample (90 % of the original sample), were needed for full conversion. Acetic anhydride was thereby added in a molar ratio of 1:1 with pyridine (1.04 g, 1.06 ml, 13.13 mmol), which acts as a catalyst as well as a solvent and was added in excess when necessary.

The reaction was supported by microwave assisted heating (Monowave 50; Anton Paar, Graz, Austria) for better and faster conversion. The temperature of 150°C was held for 1 minute.

The reaction was quenched with about 30 ml of 0.1 M hydrochloric acid, filtered and washed with water and HCl. The brown filter cake was dried at 50°C. The yield was 0.509 g (73.9 % with respect to lignin).

3.3.2. Silylation of lignin

For the trimethylsilylation of lignin, 0.68 g of dried lignin were dissolved in 5 ml THF in an ultra sonic bath (VWR ultra sonic cleaner) for 15 minutes. The equipment used in the following steps was flushed with nitrogen for 30 minutes to create an almost inert atmosphere. The dissolved lignin was transferred to a three necked round bottom flask with a cooler using 10 more ml of THF. The lignin solution was heated to 70°C (weak reflux) and 2 equivalents of HMDS (1.94 ml, 1.50 g, 9.28 mmol) were slowly added. The temperature was held at 70°C for at least 4 hours. Then the reaction was allowed to cool down to room temperature and the solvent was removed. The solid product was then dissolved in chloroform, transferred to another vessel and dried in the oven for 24 h. For Si3S1, 3 equivalents of HMDS were used instead of two and 0.3 equivalents of TMSCl (0.133 ml; 0.11 g; 1.05 mmol for 0.52 g lignin) were added as a catalyst. The yield was 0.859 g (84 % with respect to lignin).

3.4. Film preparation

Solutions of lignin and lignin derivatives were subject to spin coating. Lignin is not fully soluble in water and the most organic solvents, but is readily dissolved at higher pH. Therefore sodium hydroxide and ammonium hydroxide solutions were used as solvents for spin coating of lignin. DMF, chloroform and THF were used to prepare solutions of AcL, while SiL was dissolved in chloroform. All solutions were filtered through a PVDF filter (CHROMAFIL$^{(R)}$Xtra; PVDF-45/25; 0.45 µm; Carl Roth) prior to spin coating. 40 µl of solution per square centimeter were statically spin coated for 60 s.

The spin coating parameters (speed and acceleration) were varied (1000 rpm, 1500 rpm, 2000 rpm and 4000 rpm) to find the parameters yielding the thinnest films at a coating time of 60 seconds. In all further experiments an acceleration of 4000 rpm and a rotation speed of 4000 rpm were used.

The concentration of lignin and AcL in the spin coating solution was varied between 0.1 and 2.0 wt%. In addition a study on film thickness of AcL and SiL was done with concentrations between of 5 mg/ml, 10 mg/ml, 20 mg/ml, 35 mg/ml and 50 mg/ml.

3.5. Patterning

3.5.1. Illumination

For the illumination experiments a Heraeus germicidal low pressure UV lamp (GPH212T5L/4; 10 W; 425 mA; 30 V; 2.7 W UVC output; 26 µW UVC/cm2 at 1 m) and a SolarConstant MHG 4000 from Atlas (4000 W; Global radiation similar CIE 85 spectrum) were used. The distance between the lamp and the sample was about 10 cm for the Heraeus lamp and 30 cm for the SolarConstant. Illumination times were varied between 2 and 60 minutes.

For the cross linking experiments a Hamamatsu LIGHTNINGCURE UV-LED spot light source lamp was used.

3.5.2. Developement

For developing the substrates were immersed into chloroform and washed for 10 min. Afterwards the films were rinsed with deionized water to dissolve salts and remove leftovers of the non-recovered film.

3.6. Characterization methods

3.6.1. GPC

For the determination of the molecular mass of a polymer, gel permeation chromatography was used. The investigation was done with a WGE SEC by Dr. Bures (112 µl injection volume; A_2=0.5 µl mol/g^2; duration 30 min; eluent THF; flow rate 1.0 ml/min). For the separation two 5 µ MZgel-SDplus linear columns by MZ Analysetechnik equipped with a refractive index as well as a UV detector were used. Prior to the measurement, the lignin sample needed to be acetylated (3.3.1) to be soluble in THF.

3.6.2. Profilometry

For the film thickness and roughness determination a Dektak XT stylus profilometer from Bruker was used with Vision64 as a software for data processing. Per measurement 1000 µm were scanned over a time of 10 s with a resolution of 0.33 µm/pt and a range of 6.5 µm. The stylus had a radius of 12.5 µm and the stylus force applied was 3 mg. All measurements were acquired by single acquisition and repeated at least 6 times.

3.6.3. ATR-IR spectroscopy

Attenuated total reflection infra red spectra were obtained with a Alpha FT-IR spectrometer (from Bruker, Billerica, USA) with the APLHA's Platinum ATR single reflection diamond ATR module and the software OPUS (version 4.0) was used for data acquisition and processing. 48 spectra were collected from 400 to 4000 cm^{-1}. Cleaned, reused SPR gold slides (from bioNavis,Tampere, Finland) were used as substrates. Individual adaptive baseline correction and standardization by peak area was done with Spectragryph (version 1.2.9). The data were normalized for a better comparability using the aromatic skeleton vibration peak at 1600 cm-1.

3.6.4. UV-VIS spectroscopy

UV-VIS spectra of the photo acid initiators were recorded from 210 to 500 nm with a Lambda 25 spectrometer (from Perkin Elmer, Waltham, U.S.) in SUPRASIL QS quartz cuvettes (from Hellma Analytics, Müllheim, Germany).

3.6.5. Contact Angle measurements

To determine the surface energy of the thin films a contact angle measurement system (DSA100) from Krüss (Hamburg, Germany) was operated with a drop volume of 3 µl. The static contact angles of water and diiodo-methane were used for the calculation of the free surface energy. The contact angle was fitted with the ellipse-fitting method and averaged over at least 8 measurements on three samples. Free surface energy was calculated according to the assumptions of Owen-Wendt-Rabel-Kaelble (OWRK).

3.6.6. AFM

AFM images were recorded with a Bruker Dimension FastScan in tapping mode. The cantilevers were of the FastScan-A type with a spring constant of 18 N/m and a resonance frequency of 1400 kHz. The scan rate was 20 µm/s for 10x10 µm images and 8 µm/s for smaller images. All experiments were carried out at ambient conditions. For data evaluation NanoScope Analysis 1.5 from Bruker was used.

3.6.7. ^{1}H and ^{31}P-NMR spectroscopy

Phosphorus-31 NMR measurements were carried out with a Varian 500MHz NMR instrument after in-situ phosphorylation according to a procedure by Argyropoulos [59], and further developed by Monatil-Rivera et al. [60]. The doubled amount of solution was produced using 60 mg of lignin sample, 100 µl of 2-Chloro-4,4,5,5,tetramethyl-1,3,2-dioxaphospholane, as phosphitylating agent, 200 µl of a 5 mg/ml tris(2,4-pentanedionato) chromium(III) solution, as relaxation enhancer, 200 µl of a 10.85 mg/ml cyclohexanol solution, as internal standard, and filling up to 2 ml with a pyridine/deuterochloroform mixture (1.6:1 v:v). The spectra were obtained using a 500 MHz NMR by Varian with settings described in the literature [61]. Those spectra were processed and analyzed with a TopSpin software from Bruker.

^{1}H-NMR spectra of acetylated lignin were measured using a Bruker NMR with 300 MHz with 4 s delay time and 64 scans averaged. About 20 mg of sample were dissolved in 0.8 ml of $CDCl_3$ without tetramethylsilane standard. The solvent peak at 7.26 ppm [62] was used as reference.

Quantitative ^{1}H-NMR spectra were recorded as described above. All samples were dissolved in DMSO-d_6 or deuterated chloroform. Internal standardization was provided by adding 50 µl of a pentafluorobenzaldehyde standard solution (ca. 100 mg/ml) in deuterated dimethylsulfoxid or deuterated chloroform to all SiL and AcL samples and by adding a defined amount of pentafluorobenzaldehyde (between 2 and 7 mg) directly to the sample. For the analysis of all NMR spectra a MestReNova software from Mestrelab Research, S.L. was used.

3.6.8. Light microscopy

For a first evaluation of the developing step, a standard light microscope (Olympus; BX60) was used in BF mode, with a magnification of 2 and the lens 5x/0.13.

4. Results and Discussion

4.1. Derivatization of lignin

Derivatization is a decent way to modify the solubility of a molecule. Lignin is a large biopolymer and, despite a huge amount of hydroxyl groups, mostly insoluble in water and most organic solvents. By introducing more hydrophobic groups into the molecule via substitution of hydroxyl groups with either acetyl or silyl groups, the polarity can be decreased. The resulting AcL and SiL are readily soluble in common solvents such as chloroform or THF.

4.1.1. Acetylation

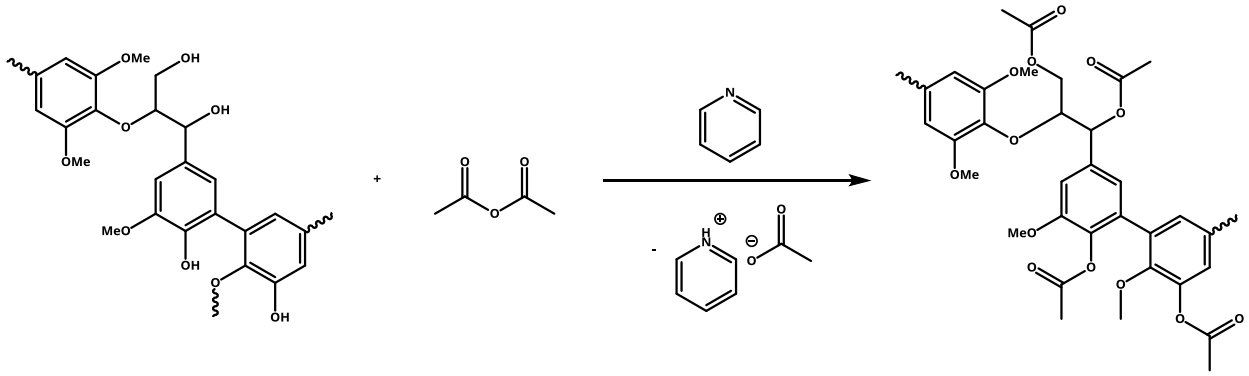

Figure 13: Lignin acetylation with acetic anhydride using pyridine as solvent and catalyst.

Acetylation of lignin was the first choice of derivatization (Figure 13), as it can be directly used for GPC analysis and a procedure has already been established [63]. However the amount of acetic anhydride added was increased from 1.6 to 2.5 equivalents due to incomplete turnover at lower ratios. In general, microwave assisted heating provides a huge advantage concerning the reaction time compared to conventional acetylation reactions. While the acetylated product can be obtained after about 20 minutes (5 min microwave reaction plus workup) using a microwave, the reaction takes at least 24 hours and needs more extensive workup using conventional methods running at room temperature [63,64].

The equivalents of acetic anhydride were calculated in respect to the amount of hydroxyl groups in the lignin, which were previously determined in a ^{31}P-NMR analysis. However, this was not successful for all four samples due to insufficient

solubility in the necessary solvent for phosphitylation. Samples with unknown hydroxyl content were assumed to contain about 10 mmol/g OH-groups and 10 wt.% of water.

The completeness of the turnover was verified with ATR-IR measurements of the dried powders (Figure 14). The IR band at 3600-3000 cm^{-1} resulting from O-H stretching disappeared during the reaction, as the hydroxyl groups were substituted by acetyl groups. On the other hand the C=O band is increased in intensity as acetyl groups are introduced into the molecule. The resulting bands could be assigned at 1760 to 1740 cm^{-1} for aromatic and aliphatic acetyl groups, respectively [65]. At 1190 cm^{-1} a band originating from the C-C-O stretching of the newly introduced saturated ester was observed. In addition, the absorption of the band at 1370 cm^{-1} increased, which was assigned to C-H bending in CH_3-group (Table 2).

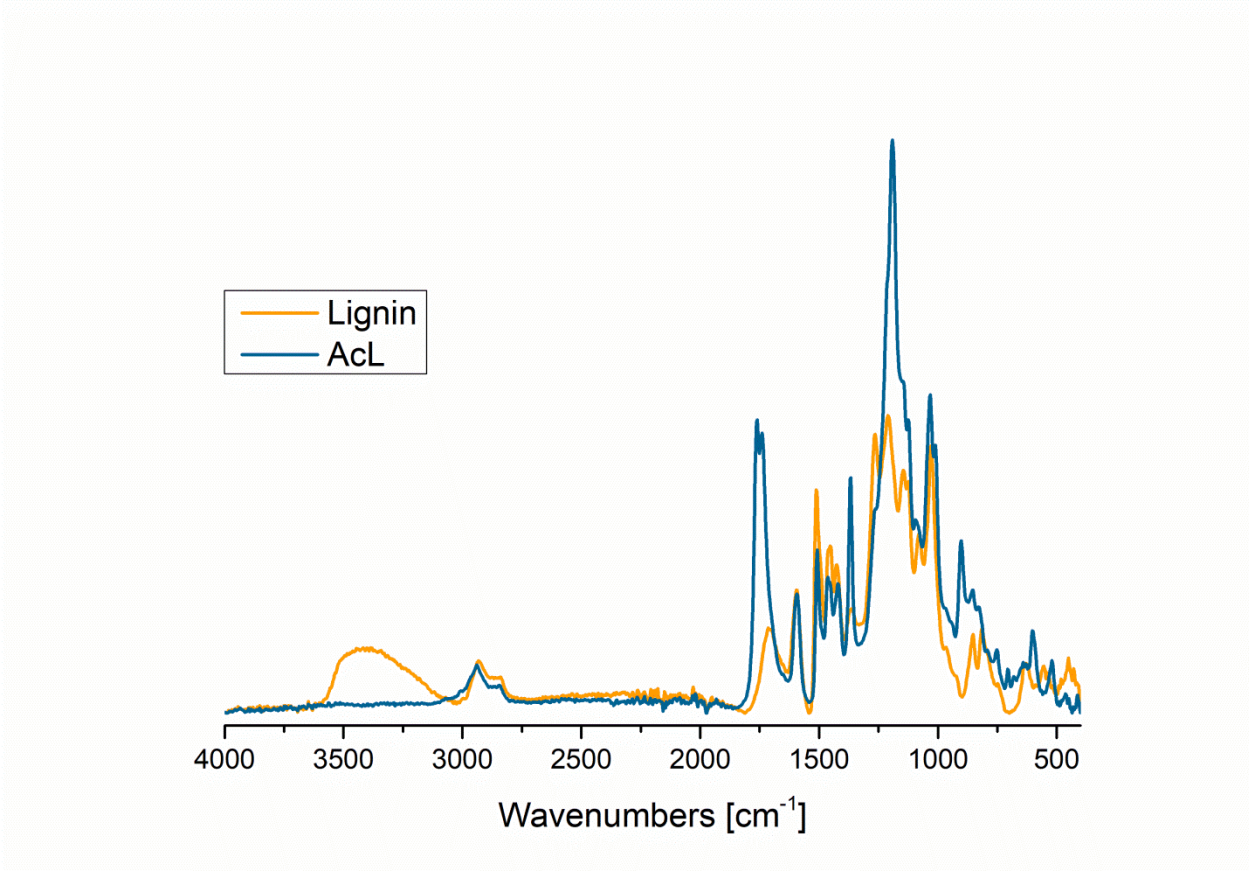

Figure 14: ATR-IR spectra of lignin (S5; orange) and acetylated lignin (Ac1S5; blue).

Table 2: Assignment of the ATR-IR signals

Signal [cm^{-1}]	Assignment	Source
3600 - 3000	O-H stretching (phenolic and aliphatic)	[1,66]
3200 - 2800	C-H stretching (CH_2 and CH_3)	[1,66]
1760 - 1740	C=O stretching from saturated esters (aromatic and aliphatic)	[65,66]
1690 - 1680	C=O stretching (aromatic; conjugated; nonconjugated)	[1,65,66]
1600 - 1590	aromatic ring C=C stretch (aromatic skeletal vibrations)	[1,65,66]
1510	aromatic ring C=C stretch (aromatic skeletal vibrations)	[1,65,66]
1470 – 1450	C-H deformation in CH_3 (asymmetric)	[1,65,66]
1430	aromatic skeletal vibrations	[1]
1370	C-H deformation in CH_3 (symmetric)	[1,65]
1270 - 1216	C-O-C and C-C-O stretching; G ring breathing	[1,65–67]
1254	CH3 umbrella mode (-TMS)	[66]
1190	C-O stretch of acetyl group (and other esters)	[1,68]
1140 - 1120	C-H in-plane deformation	[1,37,67]
1080	C-O stretch of sec. alcohols and sat. esters	[66,67]
1030	C-O-C stretch of aromatic ethers	[65]
850	C-H out-of-plane deformation (aromatic)	[1,67]
840	CH3 rocking (-TMS)	[66]
750	CH3 rocking (-TMS)	[66]

The conversion was monitored by 1H-NMR analysis, showing clear signals for phenolic and aliphatic acetyl groups at 2.34 and 2.11 ppm, respectively (Table 3; Figure 15). (note: NMR spectra of polymers, especially biopolymers show less distinct peaks than smaller molecules due to the various, slightly different environments of the examined atoms).

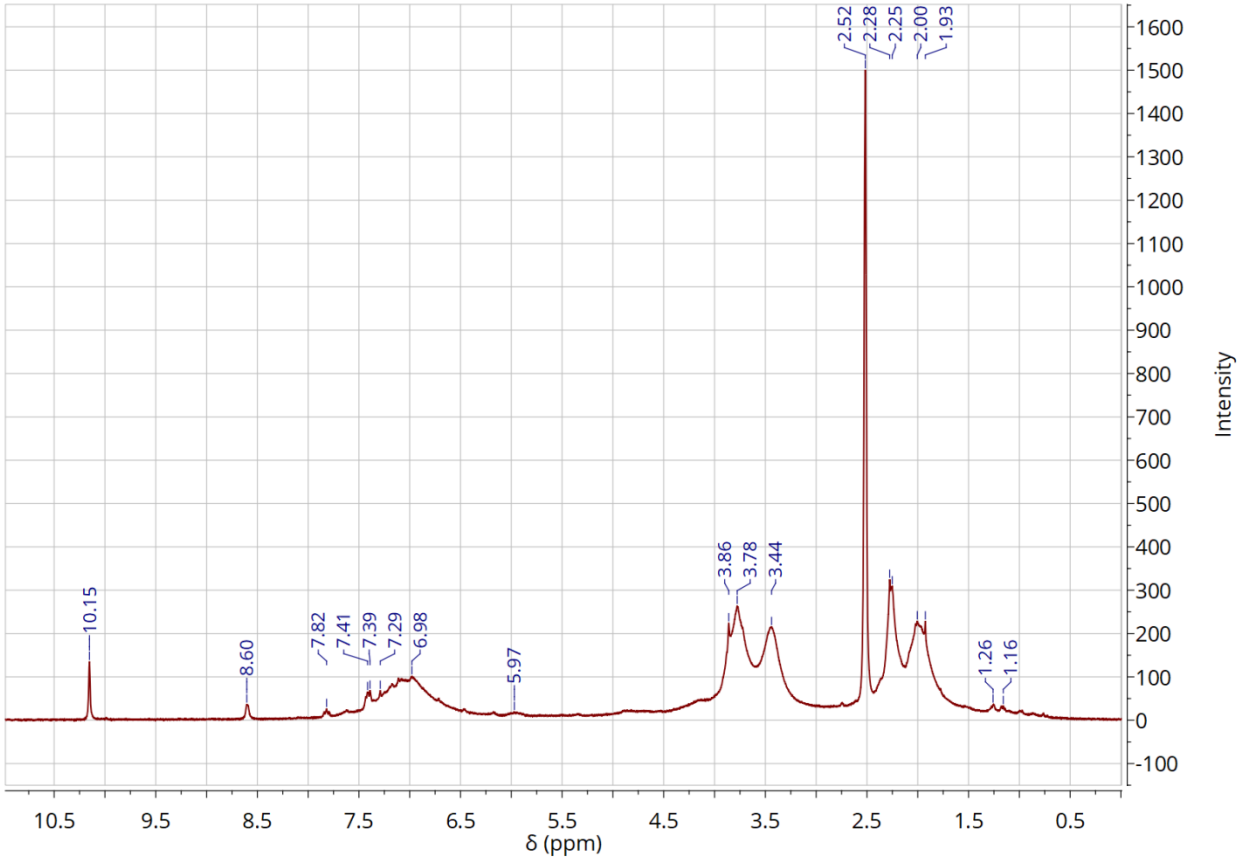

Figure 15: Quantitative 1H-NMR spectrum of Ac1S1.

Table 3: Assignment of the NMR-signals

Signal [ppm]	Assignment	Source
10.15/10.27	internal standard (in DMSO-d6/chloroform-d)	[x]
9.25 – 8.50	-OH	[x]
8.9 – 8.6	unknown	
7.5 – 6.0	aromatic H-	[1]
7.26	chloroform (solvent)	[62]
6.0 – 4.0	aliphatic H-	[8,69]
5.3	aliphatic -OH	[x]
3.9 – 3.6	MeO-	[8]
3.37	water (contaminant)	[62]
2.61	H on C-ß in acetylated ß-1 and ß-ß substructures	[69]
2.52	DMSO (solvent)	[62]
2.3	aromatic acetyl groups	[1]

Signal [ppm]	Assignment	Source
2.0	aliphatic acetyl groups	[1]
2.0 – 0.5	CH contaminants	[1]
0.5 - -0.5	TMS-	[8]
0.00	TMS standard (only in chloroform)	

[x] from ^{1}H-NMR signal estimations in ChemDraw

4.1.2. Silylation

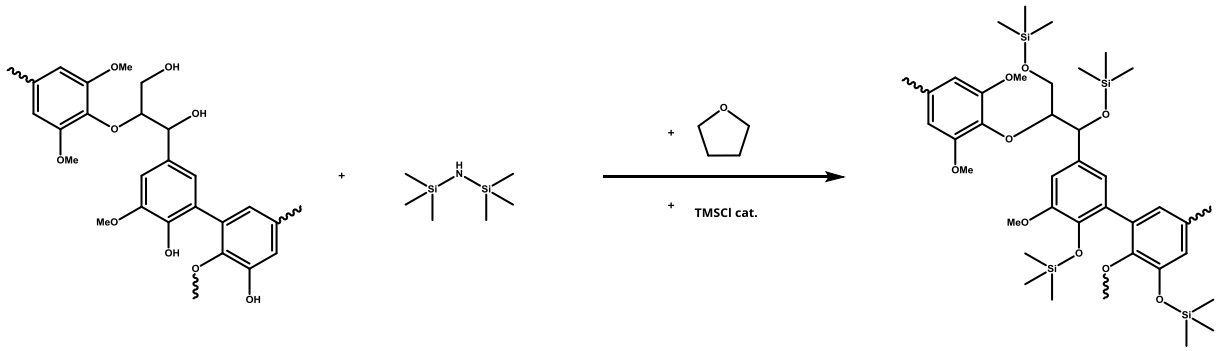

Figure 16: Silylation of lignin with hexamethyldisilazane in THF using chlorotrimethylsilane as catalyst.

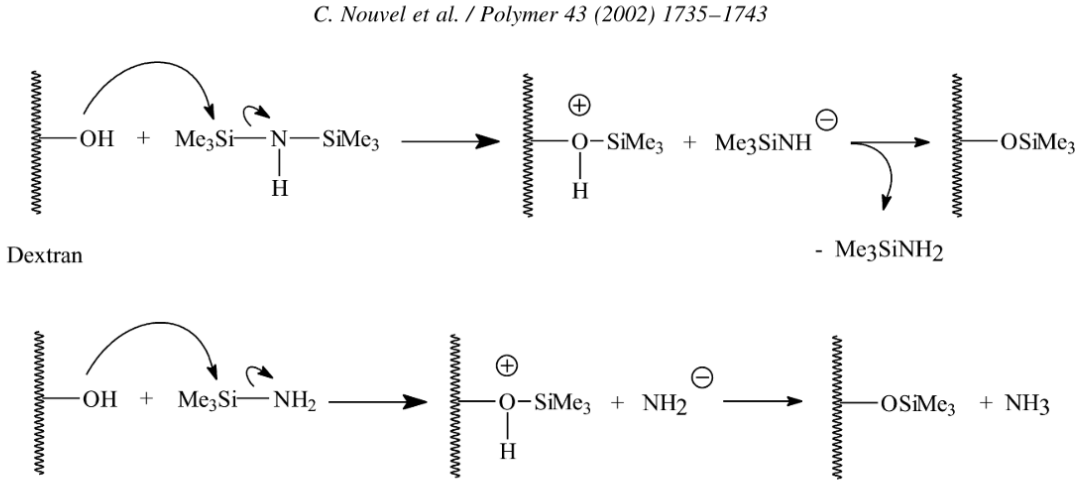

Figure 17: Mechanism of a lignin silylation of dextran with HMDS [70].

Silylation of lignin by introducing trimethylsilyl groups provides a second way of derivatization with a different way of regenerating lignin in a further step (Figure

16; Figure 17). The silylation was based on previously published procedures on various substrates (from cellulose to dextran) using different silylating agents (HMDS, TMSCl) and catalysts [8,70–72]. In the first trial 2 equivalents of HMDS were added under mild conditions as the reaction was only heated to 40°C for 2 hours. The product was then precipitated via addition of 50 ml water, separated by centrifugation and dried at 60°C over night. The conversion of the lignin was monitored using ATR-IR spectroscopy as well as ^{1}H-NMR spectroscopy, but showed incomplete turnover. Therefore the reaction conditions were optimized by adding more HMDS (3 eq.) and 0.3 equivalents of TMSCl as a reaction enhancer. The mixture was heated to 70°C for 4 hours, cooled to room temperature and the solvent was allowed to evaporate over night. When TMSCl was added the evolution of white fume was observed. This might be due to the formation of ammonium chloride (NH_4Cl) from the ammonia produced in-situ from HMDS (Figure 17) with subsequent evolution of HCl from TMSCl upon reaction with hydroxyl groups.

The conversion was checked by ATR-IR spectroscopy (Figure 18). The spectra indicated a reduction of the itensity of the hydroxyl band at 3600 -3000 cm^{-1}. The band associated to C-H stretching at 2950 cm^{-1} increased due to additional CH_3 groups at the TMS-groups and there are Si-CH_3 vibrations visible at 1254, 840 and 750 cm^{-1} (see Table 2). In further experiments the OH-stretch as well as the TMS-vibration bands was used to evaluate the regeneration process.

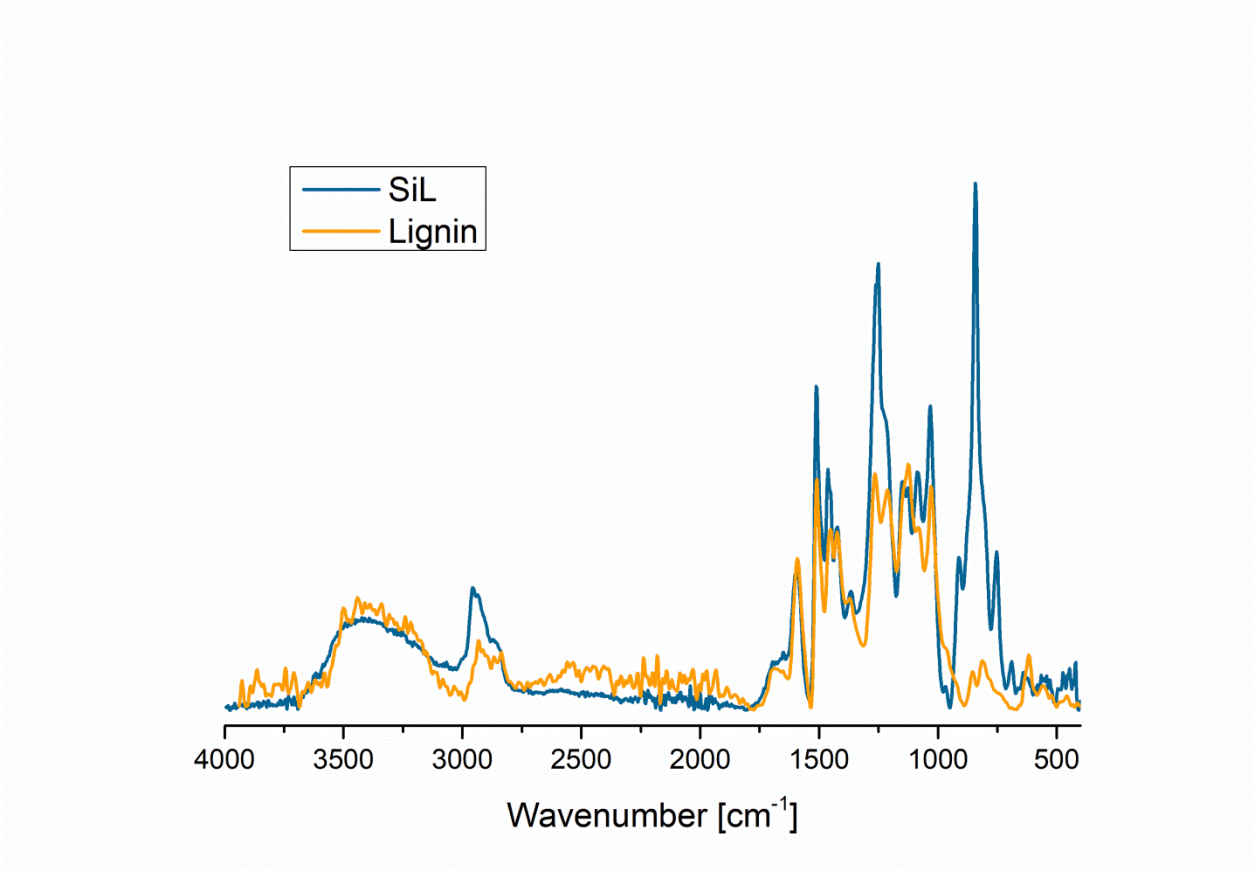

Figure 18: ATR-IR spectra of lignin (S1; yellow) and silylated lignin (Si1S1; blue).

In 1H-NMR spectroscopy the introduction of the TMS-group was proven by the appearance of peaks at 0.2 ppm (-OTMS) and 0.0 ppm (TMS) (see Table 3; Figure 19).

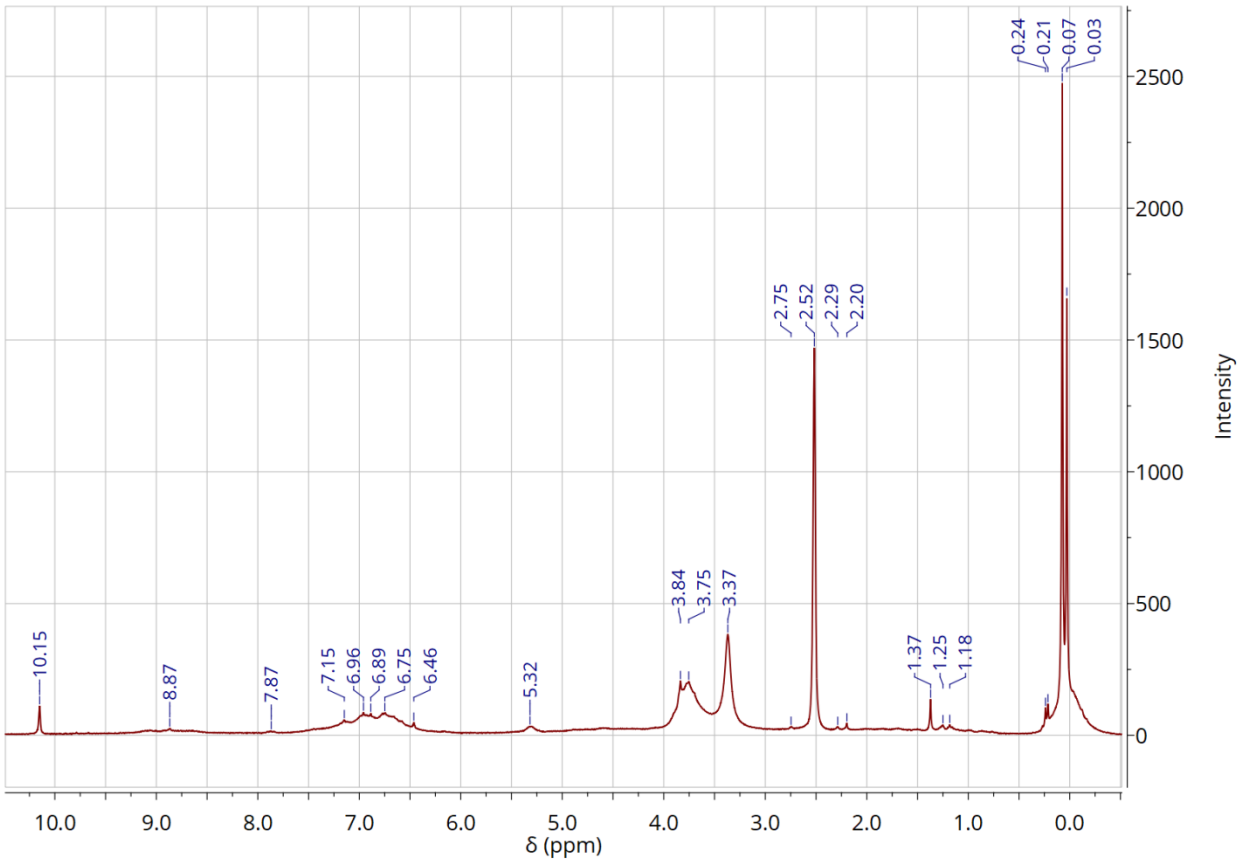

Figure 19: Quantitative 1H-NMR of Si3S1.

4.2. Characteristics and properties of the lignin samples

4.2.1. Solubility

Lignin is insoluble or only partially soluble in water and the most common organic solvents [8,55]. This can be utilized for fractionation processes [73] and is the foundation for the solubility differences needed for micro-structuring. By introduction of a more hydrophobic functionality to the molecule, the solubility properties change drastically. Silylated lignin (SiL) and acetylated lignin (AcL) are well soluble in chloroform, THF and acetone, whereas kraft lignin is insoluble in these solvents.

The solubility was tested for all lignin samples and selected silylated and acetylated samples. For the evaluation, 30 mg of dry, (powder) samples were added to 1 ml of solvent.

Table 4: Solubility behaviour of lignin and lignin derivatives. – insoluble; +/- mostly insoluble; + mostly soluble; +++ completely soluble.

	H_20	Amv	THF	$CHCl_3$	DMF	EtOH	CH_3CN	Et2O	Acetone
S1	-	+++	-	-	+++	+/-	-	-	+/-
S3	+/-	+++	-	-	-	-	-	-	-
S4	-	+++	-	-	+/-	-	-	-	-
S5	-	+++	+++	-	+++	-	+/-	-	+/-
Ac1S1	-	-	+++	+++	+++	-	+++	-	+++
Ac1S3	-	+/-	+++	+++	+++	-	+++	-	+++
Ac1S4	-	-	+++	+++	+++	-	+++	-	+++
Ac1S5	-	-	+++	+++	+++	-	+++	-	+++
Si2S1	-	-	+++	+++	+++	+/-	+++	-	+++
Si1S5	-	-	+++	+++	+++	+	+	-	+++

The herein used lignin samples exhibited quite different solubility behaviour. Evstigneev et al. [53] showed that lignin solubility was not only depending on the molecule size, as in most macromolecules. Decisive for the solubility behaviour of lignin was the number of groups accessible to solvation. Therefore, the increase of hydrophilic phenolic hydroxyl groups per phenyl propane unit should increase the solubility in aqueous sodium hydroxide solution.

This trend was confirmed by ^{1}H-NMR spectroscopy of the acetylated lignin samples. The water soluble sample (AcWL) had a high ratio of aromatic acetyl groups to aliphatic acetyl groups, while the water washed sample showed the lowest ratio (Figure 20). The other samples seemed to align with the tendency of solubility shown in Table 4. Sample S3 was partly water soluble, containing the water soluble fractions combined in AcWL and the water insoluble fractions combined in sample S4.

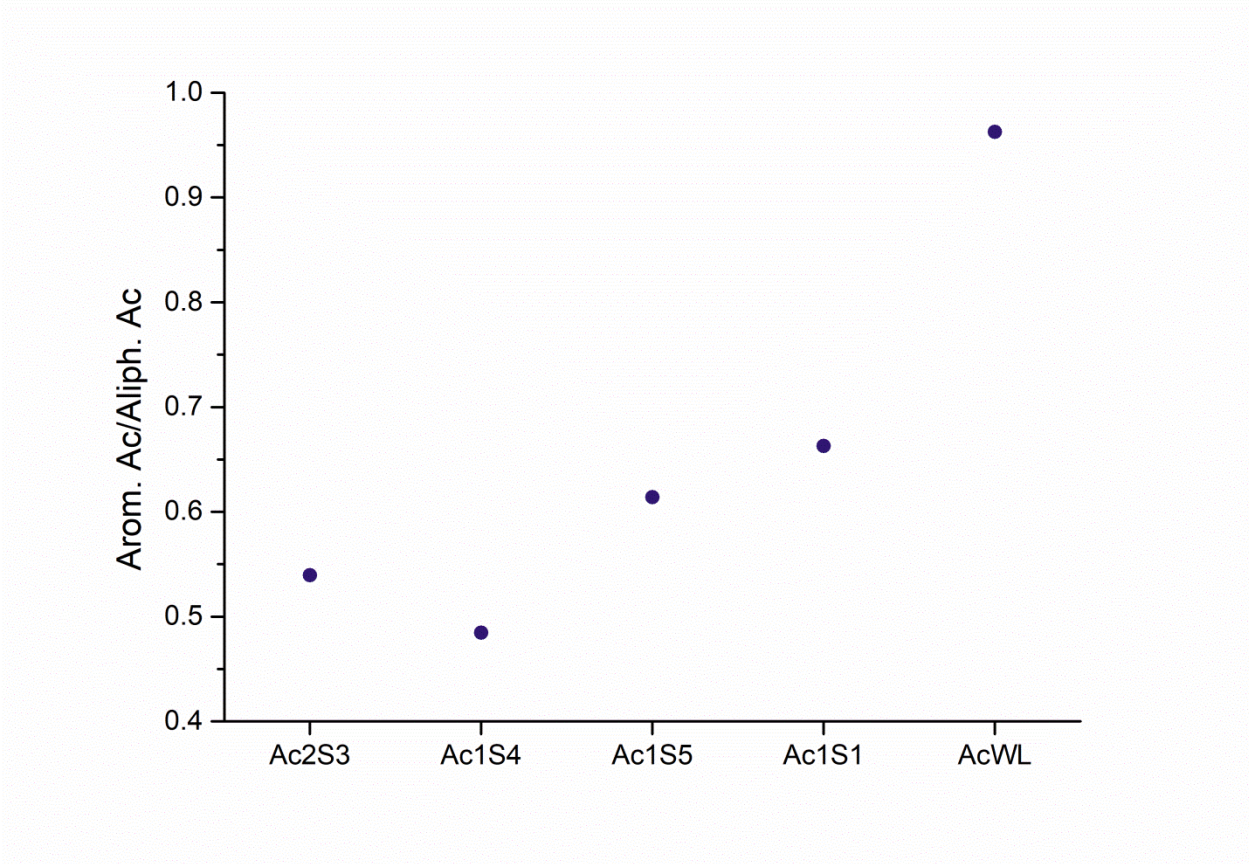

Figure 20: Ratio between aromatic and aliphatic acetyl groups in the acetylated lignin samples. Ac2S3: Pöls unwashed; Ac1S4: Pöls water washed; Ac1S5: Pöls acid washed; Ac1S1: Sigma Aldrich; AcWL: Pöls water soluble.

4.2.2. Degree of substitution

The degree of substitution of lignin was evaluated by ^{31}P-NMR or quantitative ^{1}H-NMR spectroscopy (Table 3). In ^{31}P-NMR spectroscopy, the number of hydroxyl groups was determined after phosphitylation [59] and a detailed statement on the hydroxyl and substituent positions was made. According to Buono et al. [8] there is a good correlation between ^{31}P-NMR and quantitative ^{1}H-NMR spectroscopy concerning the estimation of the number of silyl/acetyl groups, however the ^{1}H-NMR method tends to underestimate the number of functional groups.

The total amount of hydroxyl groups of S1 was determined by ^{31}P-NMR spectroscopy. The other samples could not, or not fully, be characterized by this method, as the solubility was insufficient in the required solvent.

For S1, however, a comparison with the ^{1}H-NMR spectroscopy results could be made. The results for total substituent groups from ^{1}H-NMR were adapted to the ^{31}P-NMR measurements by applying the equation 1 [8]. This makes up for the underestimation of functional groups of this method (eq. 5).

$$c(\mathrm{P-NMR}) = 0.89c(\mathrm{H-NMR}) - 0.61 \qquad \text{(eq. 5)}$$

By calculating the ratio of the acetyl or silyl groups found in ^{1}H-NMR spectroscopy and the number of OH-groups found in ^{31}P-NMR spectroscopy, the degree of substitution can be estimated [74]. The acetylation yields a degree of substitution of 81 %, while silylation leaves about half of the hydroxyl groups unsubstituted (Table 5).

Another way of estimating the degree of substitution is by comparing the number of acetylated groups with the number of silylated groups determined by ^{1}H-NMR spectroscopy, with the assumption of full acetylation of the latter. This, however, needs to be confirmed by another method (e.g., IR spectroscopy) to confirm complete disappearance of hydroxyl groups upon acetylation (Table 5).

Table 5: Total number of substituents and degree of substitution

	S1 (Sigma Aldrich)	**S5 (Pöls; acid washed)**
tot. OH-groups (^{31}P-NMR)	13.56	(1.77)[(a)]
tot. Ac-groups (^{1}H-NMR)	10.22	5.64
tot. TMS-groups (^{1}H-NMR)	5.76	5.53
Degree of Substitution [%]		
Ac/adapted P	81	-
TMS/adapted P	48	-
TMS/Ac	(56)[(a)]	98

[(a)]experiments should be repeated due to dissolution problems or no full substitution according to IR.

4.2.3. GPC and molecular mass

The molecular mass of the lignins was determined by gel permeation chromatography using THF as an eluent. Therefore, the sample was acetylated prior to the measurement to provide full solubility.

The number-averaged molar weight of all 4 samples is between 1.8 and 2.1 kDa (Table 6) which is an expected range for kraft lignins [11,12]. The *unwashed lignin (S3)* shows the lowest molecular weight. The *water washed (S4)* sample has a slightly higher molecular weight, which might be due to the leaching of smaller polymer fractions, but mainly due to the dissolution of salts. Thereby, the solubility of demethoxylated lignin is increased and it is washed out of the S4 sample. *Acid washed (S5)* lignin shows a lower molecular weight. The stand-alone sample from Sigma Aldrich (S1) shows a molecular mass of 1.9 kD. Overall, the samples S1, S3 and S5 show comparable M_n values. In combination with the solubility behaviour, this correlates with the statement, that the molecule size has no large impact on the solubility of lignins (4.2.1).

Table 6: Moleculare weight of the lignin samples

	M_n [kg/mol]	M_w [kg/mol]	M_z [kg/mol]	PDI [1]
S1 (Sigma Aldrich)	1.868	7.067	24.58	3.783
S3 (Pöls; unwashed)	1.802	5.744	17.42	3.188
S4 (Pöls; water washed)	2.108	8.602	28.56	4.080
S5 (Pöls; acid washed)	1.885	6.873	22.22	3.646

4.3. Film formation and characteristics – thickness, roughness and surface structure

In the first experiments, the aim was to produce thin films as thin as possible. Therefore acceleration and rotation speed in the spin coating process were varied between 1000 and 4000 rpm/s and 1000-4000 rpm at a constant concentration of 1.5 wt% lignin in ammonium hydroxide solution. The profilometry results showed a decreased film thickness at higher acceleration and rotation speed (Figure 21). A higher acceleration and rotation speed results in an increased amount of solution removed from the substrate by centrifugal forces. Therefore less solution is on the substrate during the drying and the films

are thinner than at lower acceleration and rotation speeds. For all further experiments 4000 rpm/s acceleration and 4000 rpm rotation speed were used in the spin coating process.

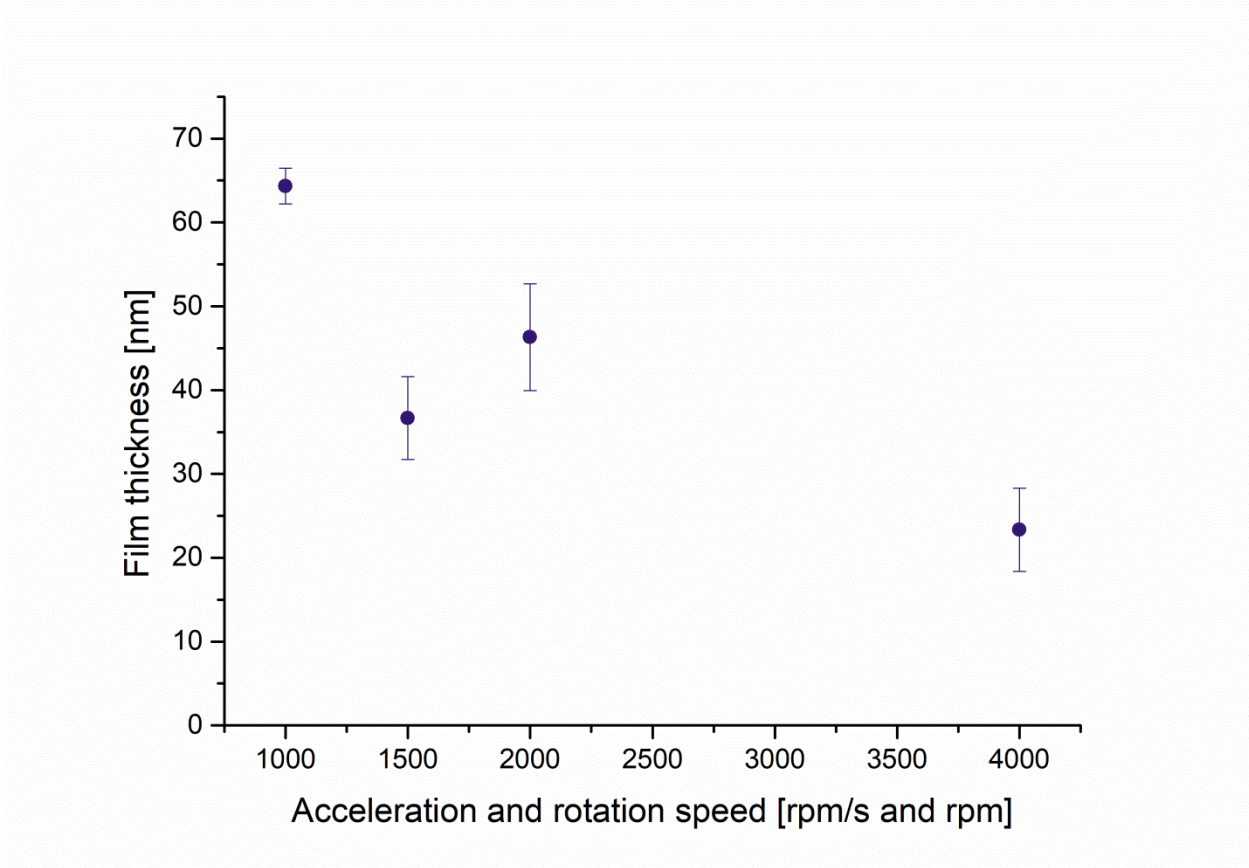

Figure 21: Lignin film thickness obtained by spin coating, varying acceleration and rotation speed.

The second step was to vary the solution concentration subjected to spin coating. Concentrations were chosen between 5 and 50 mg/ml. Immediately after the film formation an obvious difference in colour could be seen in the substrates of different concentrations (Figure 22). This colour effect is due to interferences within the lignin film when light is reflected at the interfaces, being partly reflected and partly transmitted [75]. In further experiments the colour of the films could be used for a first, quick evaluation of the film thickness. Profilometry investigations revealed a very good correlation between the film thickness and the concentration of acetylated lignins (R^2=0.997) and a good correlation for silylated lignins (R^2=0.977; with and without the addition of a photo acid generator) (Figure 23; Figure 24). At increased concentrations there

were more lignin molecules in the spin coating solution, resulting in a higher viscosity, less loss of material due to centrifugal forces and a higher proportion of molecules remaining on the substrate during solvent evaporation. With increasing film thickness also the roughness of the films increased up to 12 nm.

Figure 22: Color variations of AcL thin films directly after the spin coating process.

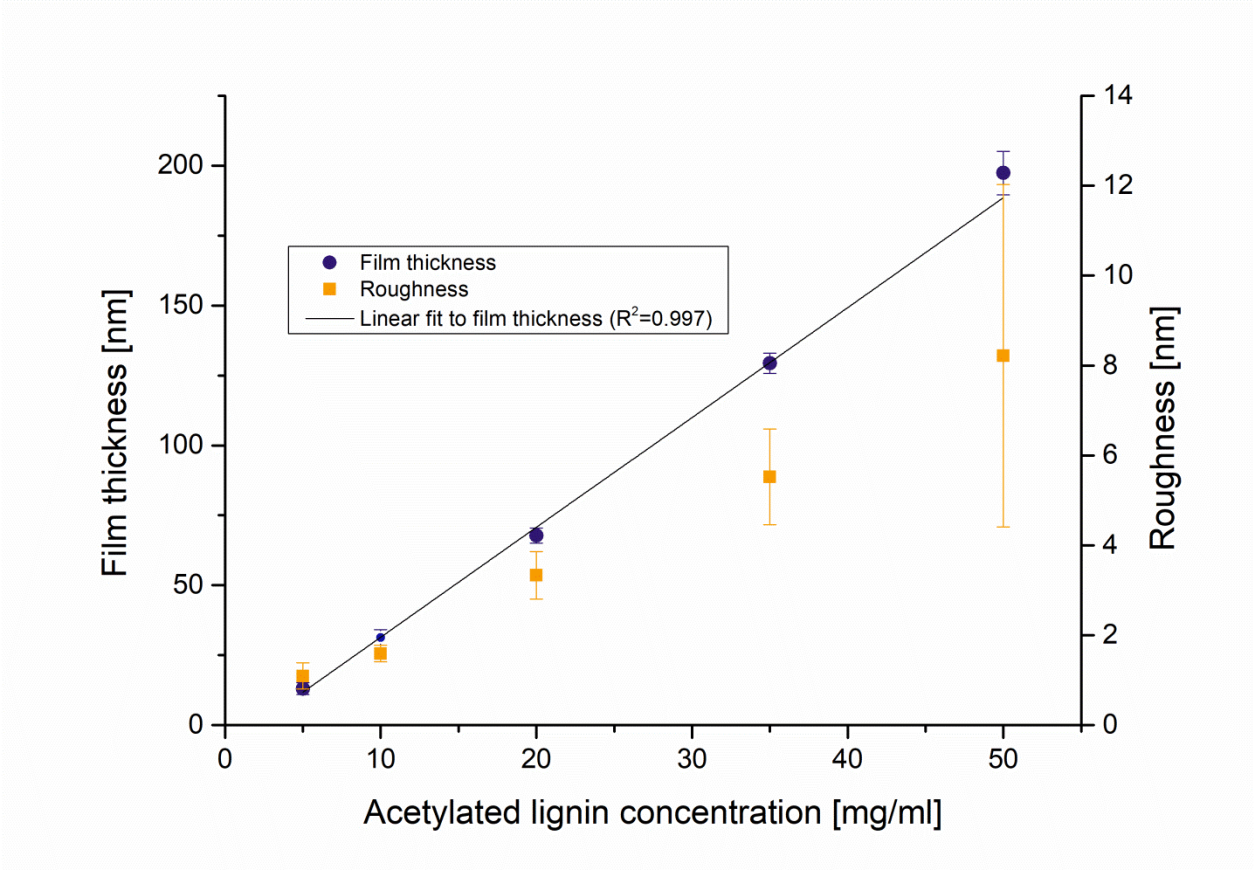

Figure 23: Mean film thickenss and roughness of acetylated lignin thin films. With a correlation of R2=0.997 for the linear fit to the film thickness.

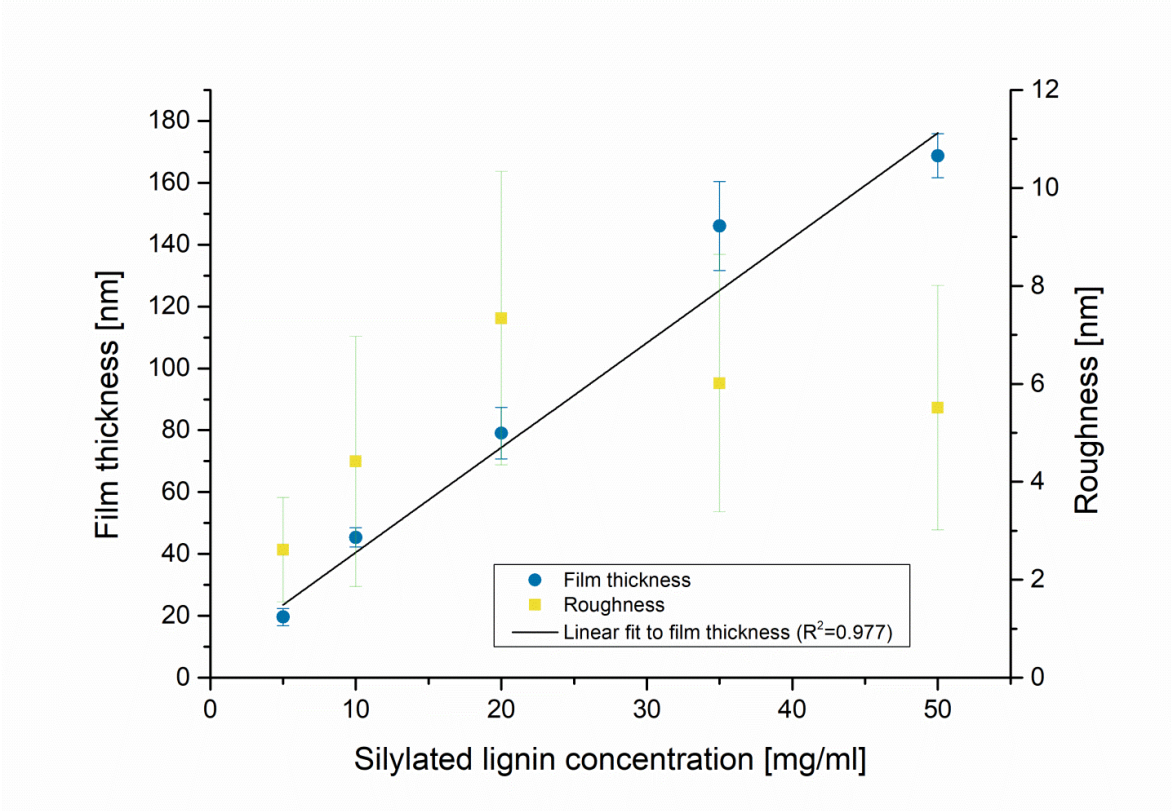

Figure 24: Mean film thickness and film roughness of silylated S1 thin films. With a correlation of R2=0.977 for the linear fit to the film thickness.

Whilst the four AcL samples showed quite similar film thicknesses (with only Ac1S2 being slightly thinner), silylated lignins differed very much in film thickness between the samples even though the mass concentration was the same in solution. This could be due to filtration effects (loss of mass and impurities whilst filtering) or different degrees of substitution between the SiL samples. However, within the same sample similar trends were observed.

To gain more information on the surface properties of lignin the surface of the lignin films was investigated by atomic force microscopy. Roughness, film thickness and especially the surface structure were subjects of the investigations.

The surface of all thin film samples was homogeneous, rather smooth and continuous over an area of at least 10 µm. The surface roughness was small and did not exceed 2 nm, except for sample Si2S1 (Figure 25: C; G). The silylated sample of S1 had a roughness of 10 – 20 nm, which is higher than expected. In both, the 5 mg/ml and the 50 mg/ml film, an agglomeration of material was observed. The aggregates had diameters of 30 – 130 nm, being slightly bigger in

the thinner film, but piled up higher in the 50 mg/ml film. The aggregation behavior in lignin thin films was previously observed by Norgren et al. [31] for pure lignin films (spin coated from 0.75 M NH_4OH). The reported size of the aggregates of 10 – 20 nm corresponds with the small, spherical aggregates found in AcL thin films (1a; 1b; 2a; 2b). Ratnaweera et al. [9] showed, that lignin can form aggregates of 700 – 1000 Å in DMSO-d. Presumably, this is also the case for SiL dissolved in chloroform. The larger aggregates in the Si2S1 sample compared to the AcL samples could be a result of the different modifications and the consequent difference in hydrogen bonding and noncovalent π-π interactions present. A higher amount of carboxyl functions, that are known to aggregate amongst each other [76], can be found in AcL and might result in a closer packing. Also the steric demand of the substituents (-OAc and –OTMS) could contribute to the size difference in the AcL and SiL aggregates. The increased aggregation behaviour correlates with the slightly lower solubility of SiL than AcL in chloroform, shown in Table 4.

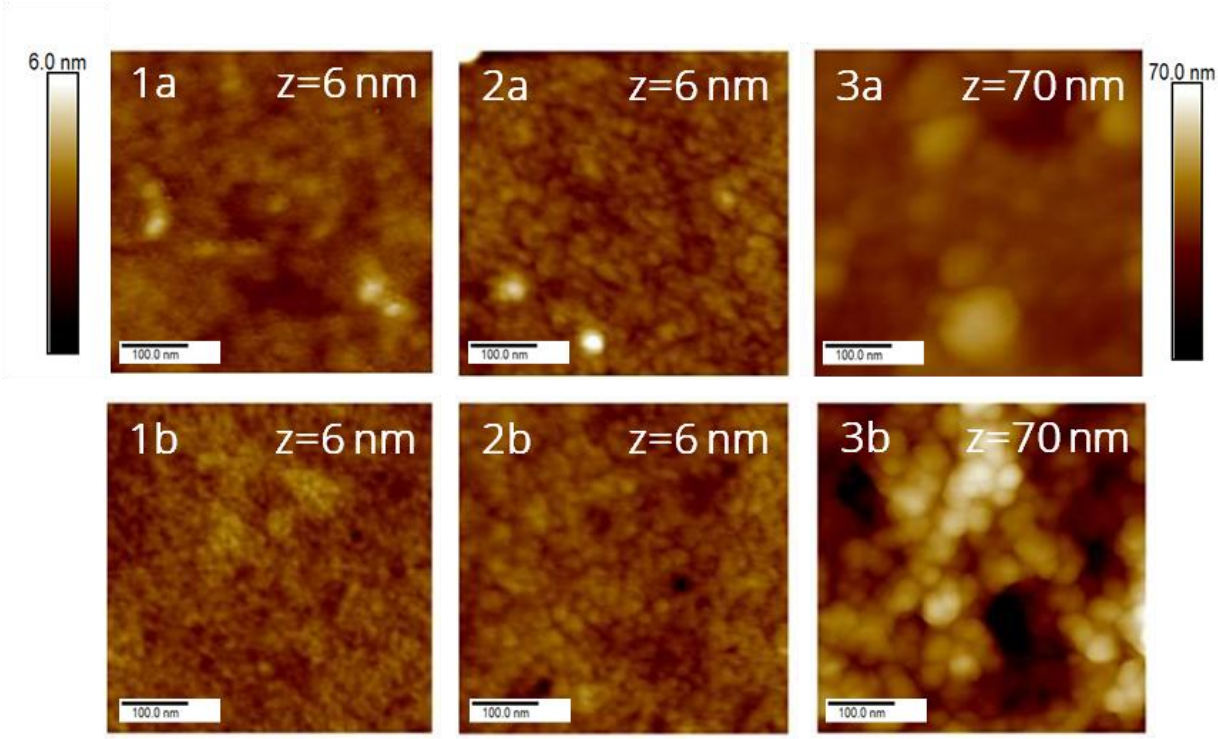

Figure 25: AFM height images of selected lignin derivatives: Ac1S1 (1a; 1b), Ac2S2 (2a; 2b), Si2S1 (3a; 3b). The films were spin coated from chloroform solutions using a concentration of 5 mg/ml lignin derivative in the upper row and 50 mg/ml in the lower row. The data scale is 500 nm x 500 nm for all images. The z-value is 6.0 nm for acetylated lignin films and 70.0 nm for silylated lignin films.

4.4. Structural changes in lignin due to regeneration or degradation processes

4.4.1. Regeneration with vapor

Depending on the protecting group used, lignin derivatives can be regenerated to lignin by re-establishing the original hydroxyl groups. Acetyl groups can be cleaved using a strong base, for instance ammonium hydroxide (NH_4OH), as the group of Rojas showed [35,36] (Figure 26). For this purpose, the substrates were placed close besides a drop of 5 ml of 28% ammonium hydroxide in a tightly sealed Petri dish. The regeneration was carried out over night and could be accelerated by increasing the temperature to 60°C. However, the regeneration to lignin was not completed, as ATR-IR spectra show (Figure 27) and no clear difference in solubility could be observed.

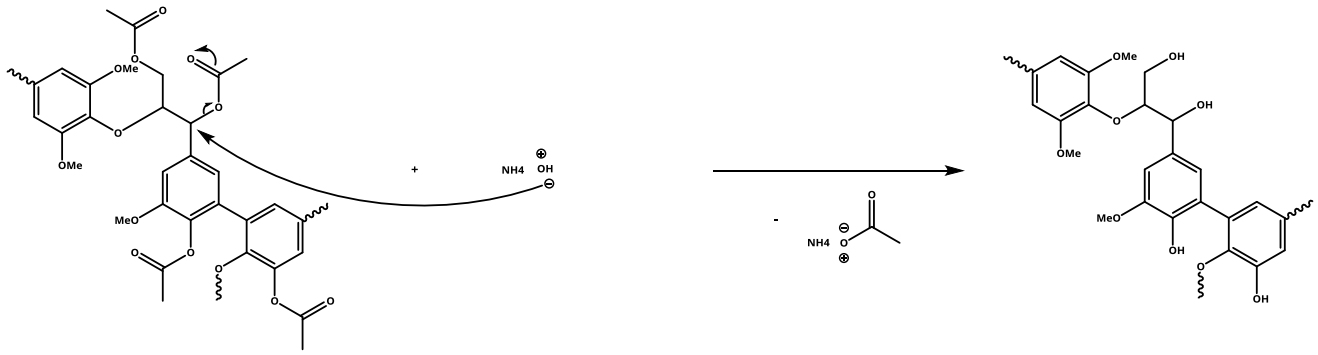

Figure 26: Scheme of the mechanism behind the regeneration of acetylated lignin with NH4OH.

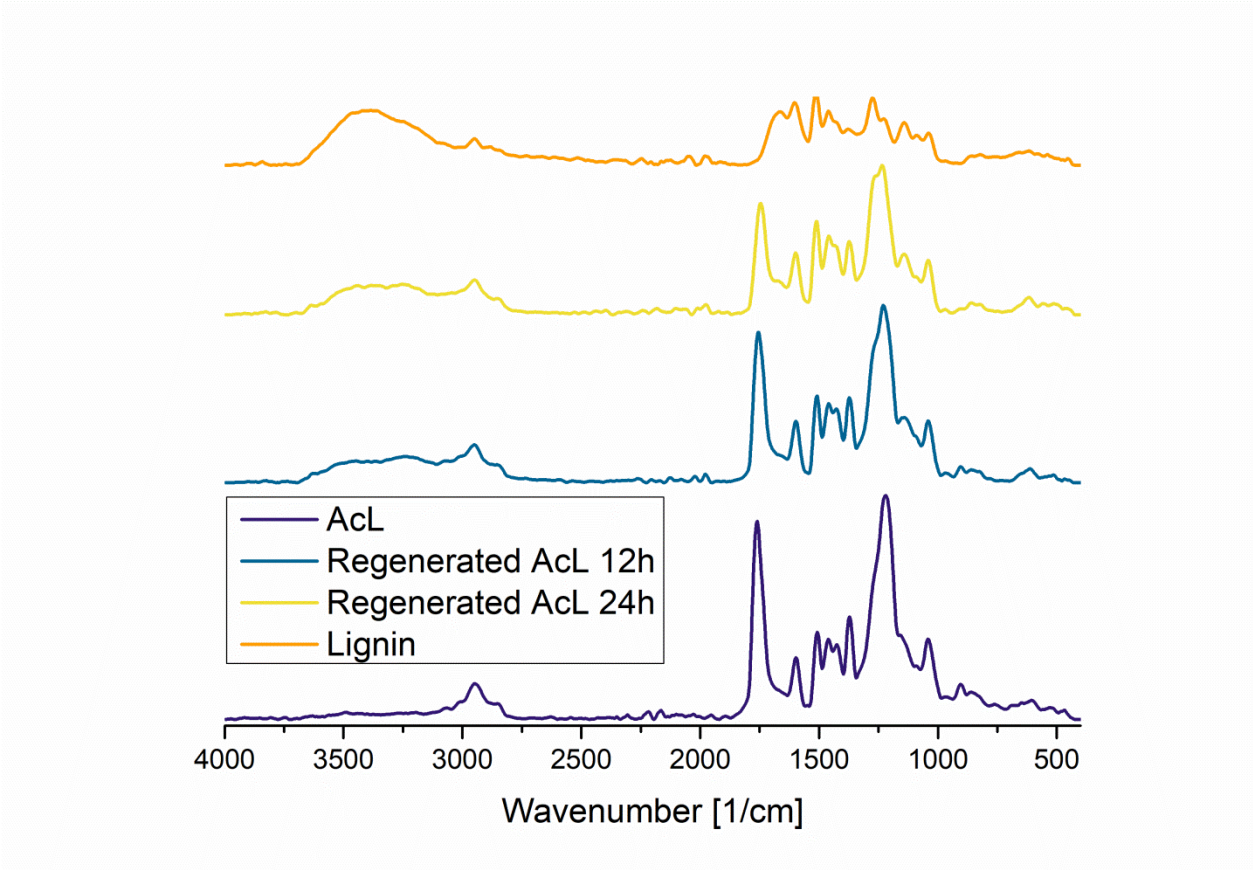

Figure 27: Time resolved ATR-IR of the regeneration of acetylated lignin.

In contrast to acetyl groups, silyl groups can be split off by strong acids (Figure 28). A vapor phase hydrolysis method is already established in cellulose chemistry for cellulose thin film applications [37,77,78]. For regeneration of lignin, the method was adapted and 3 ml of 12 % hydrochloric acid were added to the substrates in a Petri dish for 30 min.

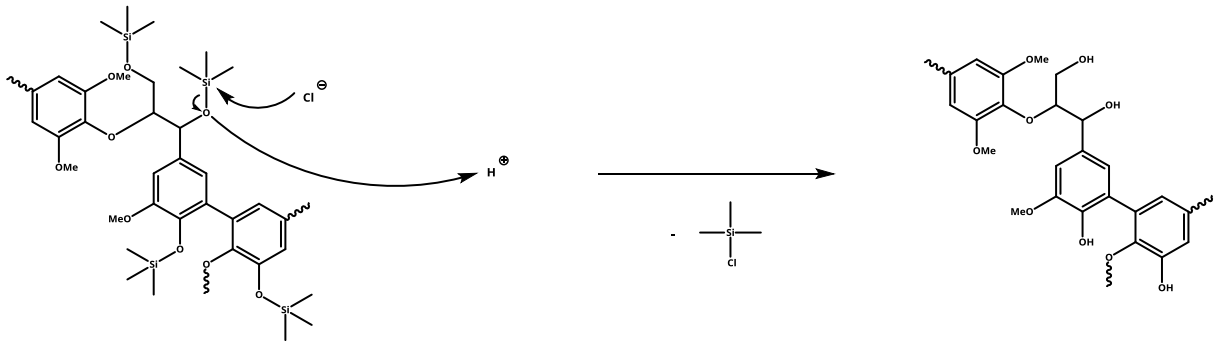

Figure 28: Scheme of the mechanism behind the regeneration of silylated lignin with hydrochloric acid.

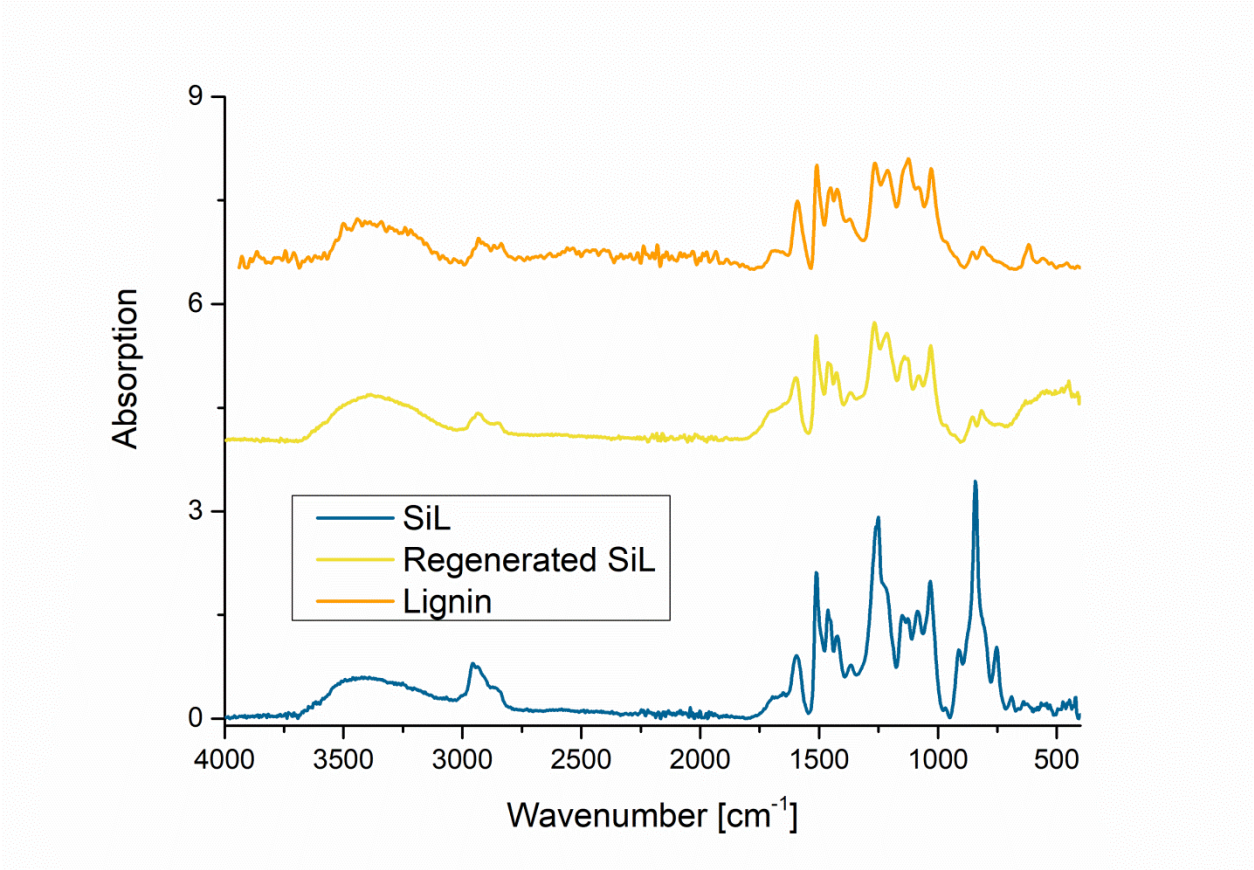

Figure 29: ATR-IR: Regeneration of silylated lignin.

The ATR-IR spectra indicated the regeneration of lignin (Figure 29). The distinct C-H and TMS- bands at 3000-2800 cm^{-1}, 1254 and 850 cm^{-1} disappeared after regeneration and a lignin spectrum is obtained.

Atomic force microscopy images visualized a change of the surface structure in Si2S1 after regeneration (Figure 30) and a growth in aggregate size from about 50 nm to 150 nm, also increasing the roughness from 19 nm to 31 nm. The thickness was just slightly reduced from 292 nm to 280 nm, according to profilometry investigations. The reduction of film thickness was expected due to the cleavage of the bulky silyl groups and concomitant reformation of hydrogen bonds, similar behavior was already reported for trimethylsilylcellulose (TMSC) before [79]. However, it was far less pronounced than in the TMSC samples due to fewer hydrogen bonds formed and the arrangement of the silyl groups. The growth in aggregates was not expected and cannot yet be explained. The altered substituents might result in a further aggregation of the regenerated lignin, as discussed before (4.3).

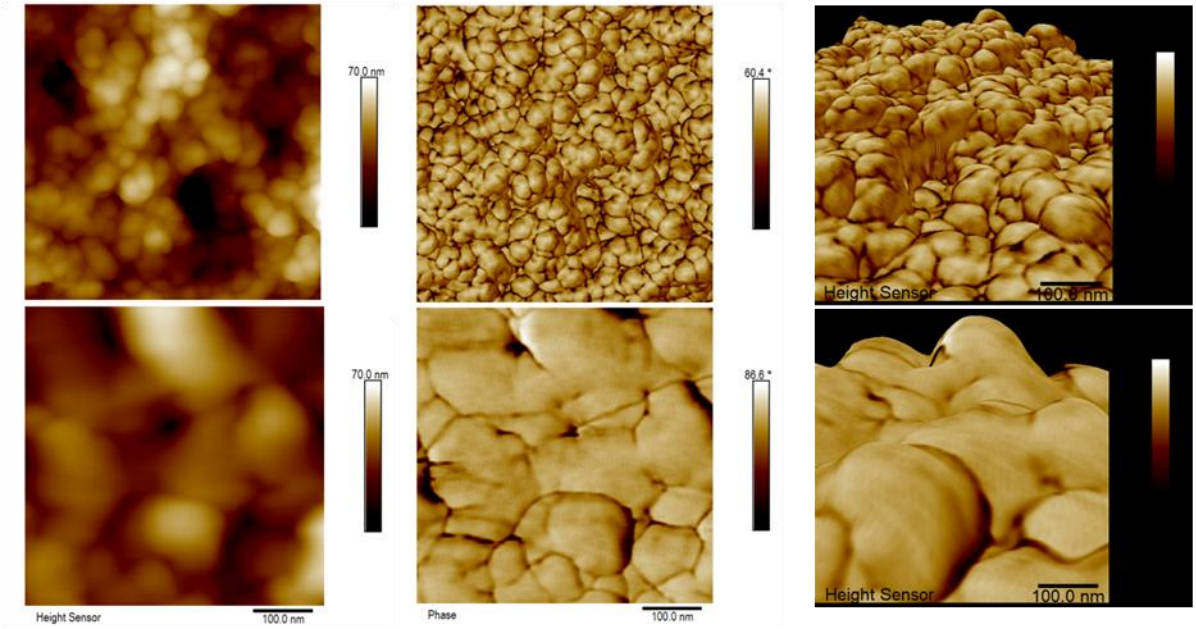

Figure 30: AFM images before (above) and after (below) regeneration of SiL (Si2S1). On the left the height image is shown, in the middle the phase and on the right an overlap of phase and height sensor to give a better resolution of the 3D image. Data scale 500 nm x 500 nm.

4.4.2. Photoregeneration - tuning of the process parameters

The regeneration of lignin via illumination of lignin derivatives was tested as described in 4.4.1. For the creation of patterned lignin surfaces a confined regeneration must be ensured. This can be obtained by photo regeneration using a photo mask.

To fine tune the process settings for a photo induced regeneration of lignin, the following parameters were altered and compared:

- A photo active component to induce regeneration of lignin.
- The amount of photo active material used.
- The lamp.
- The exposure time.
- The dark reaction time.

To evaluate the influence of these parameters the film thickness and roughness were determined with a profilometer and ATR-IR spectra were recorded to confirm the chemical conversion. In addition, AFM images and contact angle measurement were performed to follow the surface changes during the regeneration.

Photo active component

As regeneration with acid from silylated lignin gave the best SiL was mixed with a photo acid generator (PAG) to in-situ produce an acid when illuminating the substrate. Two different PAGs were tested in combination with two UV lamps.

As PAG**1**, with a main absorption peak between 300 and 360 nm, N-hydroxynaphtalimide-triflate was used (Figure 31). Upon UV-irradiation triflic acid is formed, which can cleave the TMS group via nucleophilic attack [79]. The same principle is applied when PAG**2**, namely 2-(4-Methoxystyryl)-4,6-bis(trichloromethyl)-1,3,5-triazine, is used. However PAG**2** decomposes to form HCl [40] and has its maximum absorption peak at 320 – 440 nm (374 - 381 nm according to Sigma Aldrich specifications), as well as a smaller absorption at up to 270 nm (Figure 31).

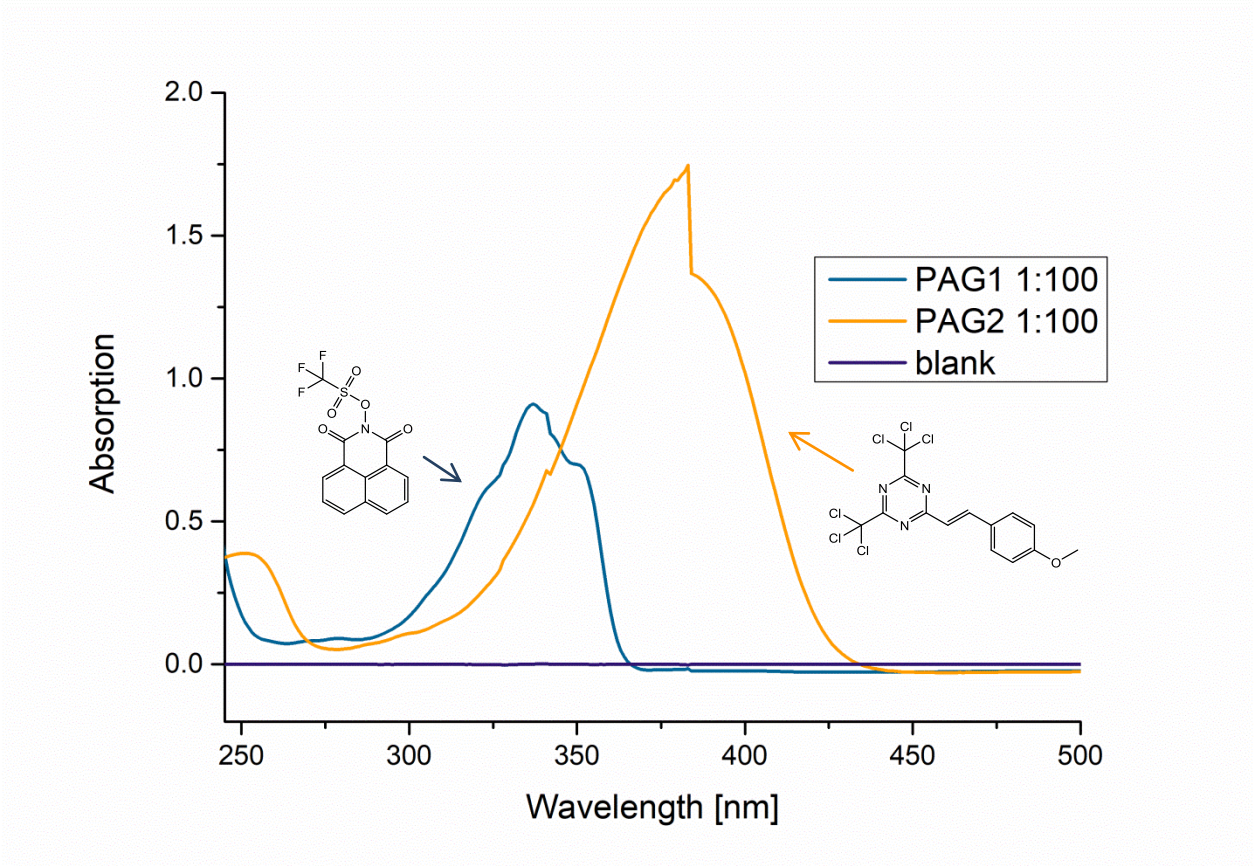

Figure 31: UV absorption spectra of the PAGs. PAG1 N-hydroxynaphtalimide-triflate and PAG2 2-(4-Methoxystyryl)-4,6-bis(trichloromethyl)-1,3,5-triazine, both measured in a 1:100 solution in chloroform.

When comparing radiation spectra of the lamps with the absorption spectra of the two PAGs one can clearly see a significant difference in overlap of the peaks and a likely difference in efficiency (Figure 32). Solely from looking at the spectral overlap it can be assumed that PAG**2** will have a higher efficiency in regeneration with both lamps. This was tested and confirmed by ATR-IR spectroscopy and profilometry measurements after illumination with the Heraeus lamp. The lignin film regenerated with PAG**2** was about 40 % thicker after washing than the one regenerated with PAG**1** and the reduction of TMS-signals in ATR-IR was more pronounced.

UV-lamps

A comparison of the influence of the two lamps was carried out by illuminating SiL samples (50 mg/ml) with 5 % of PAG**2** for 20 min and washing after 3 h of

dark reaction. The difference between distinct ATR-IR signals in the sample before and after illumination was evaluated. Thereby the Heraeus lamp showed efficiencies about twice as high as the SolarConstant lamp. Assessing from the spectral overlap of PAG**1**, neither the Heraeus lamp, nor the SolarConstant would show a good correlation with the absorption spectra thus a low efficiency for acid generation can be predicted. However, one could consider a reptile UVB lamp for further application with PAG**1**, which has a good overlap with the main absorption peak (Figure 32).

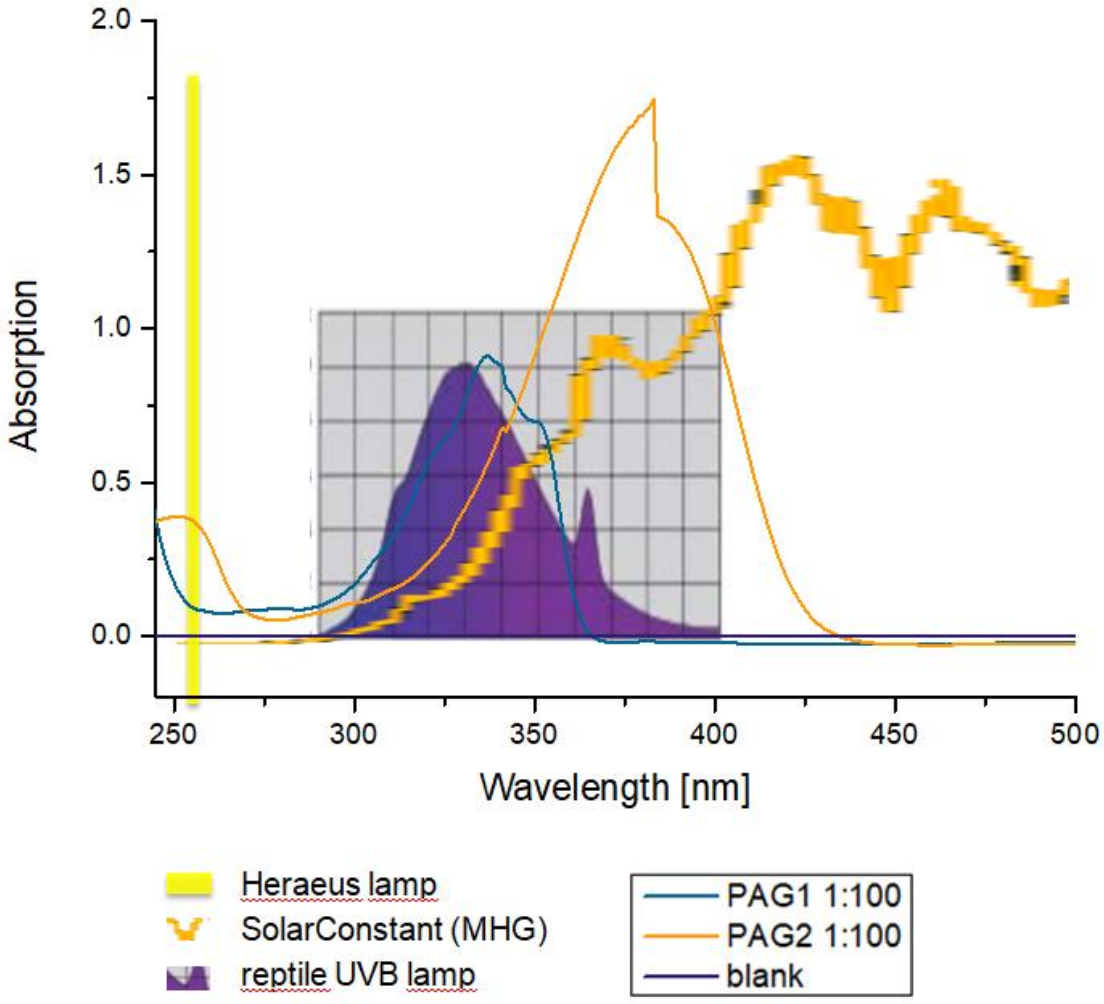

Figure 32: Comparison of lamp emission spectra with PAG absorption spectra.

PAG content

An assessment of the optimal amount of photo acid generator was carried out by varying the PAG content between 1 and 5 % (50 mg/ml SiL; 20 min illumination; 3 h dark reaction). ATR-IR and profilometry measurements showed an increase of efficiency with PAG content (Figure 33; Figure 34).

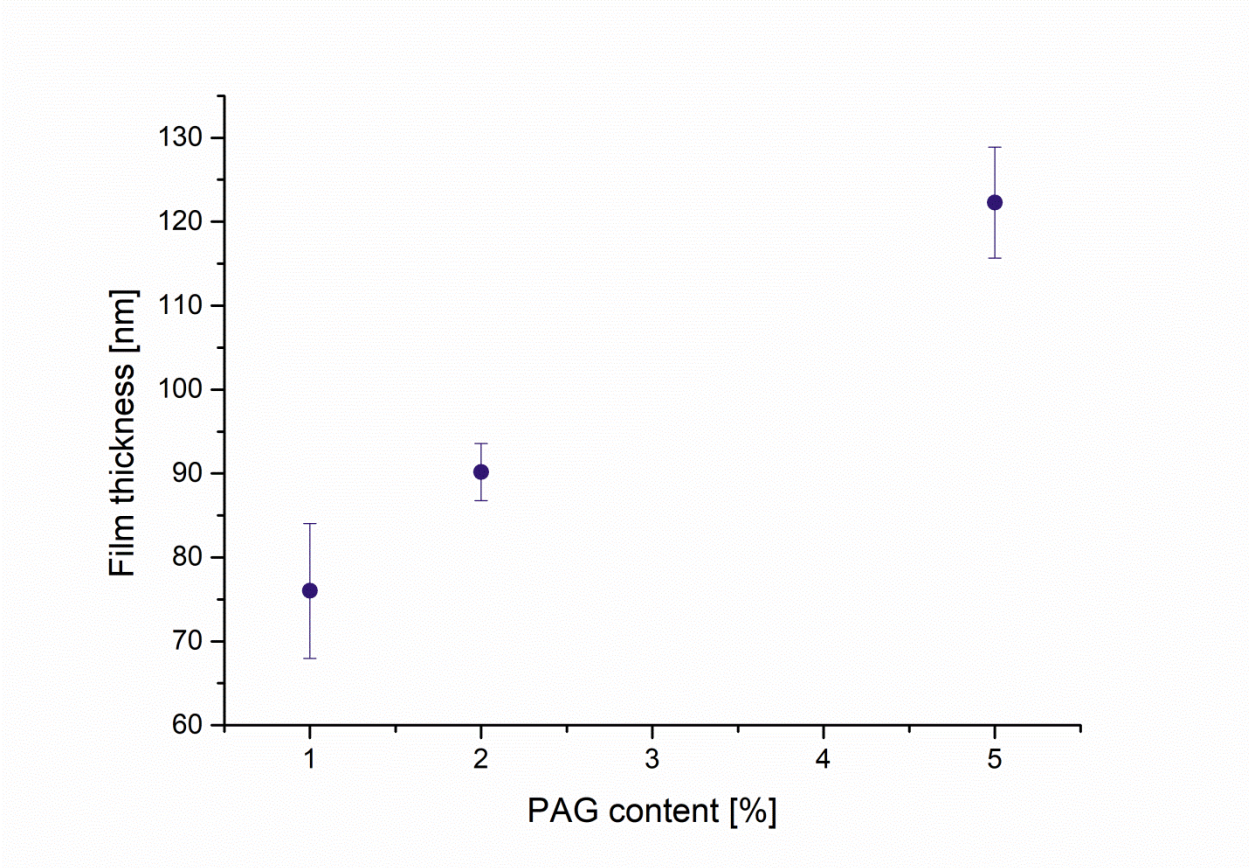

Figure 33: Thickness of the developed films with different PAG content.

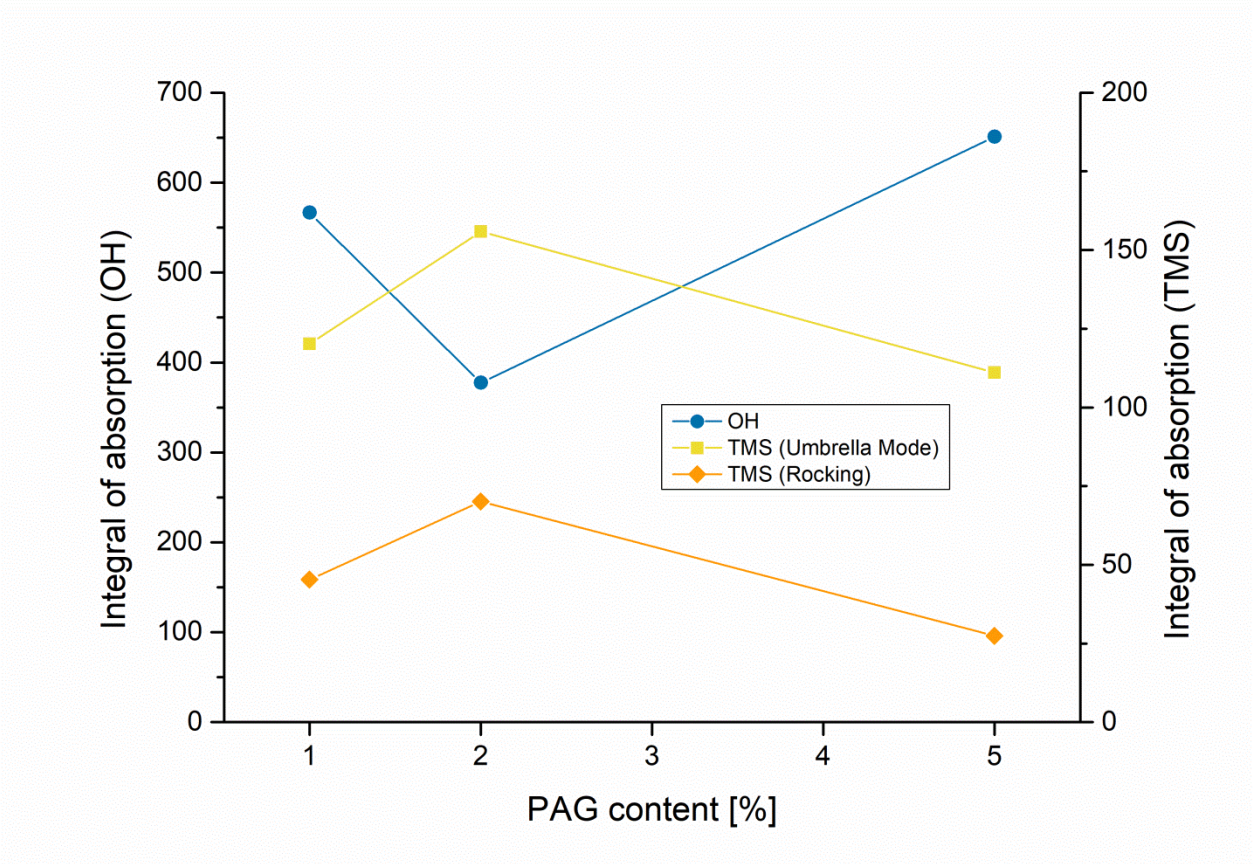

Figure 34: ATR-IR signals of OH- and TMS-groups depending on the PAG content.

Exposure time

To explore the influence of exposure time on regeneration efficiency the illumination time was varied between 1 min and 1 h. ATR-IR and profilometry showed a similar trend, albeit it was more pronounced in film thickness (Figure 35). There was a distinct increase in efficiency until 40 min of illumination time, but almost no change upon longer exposure.

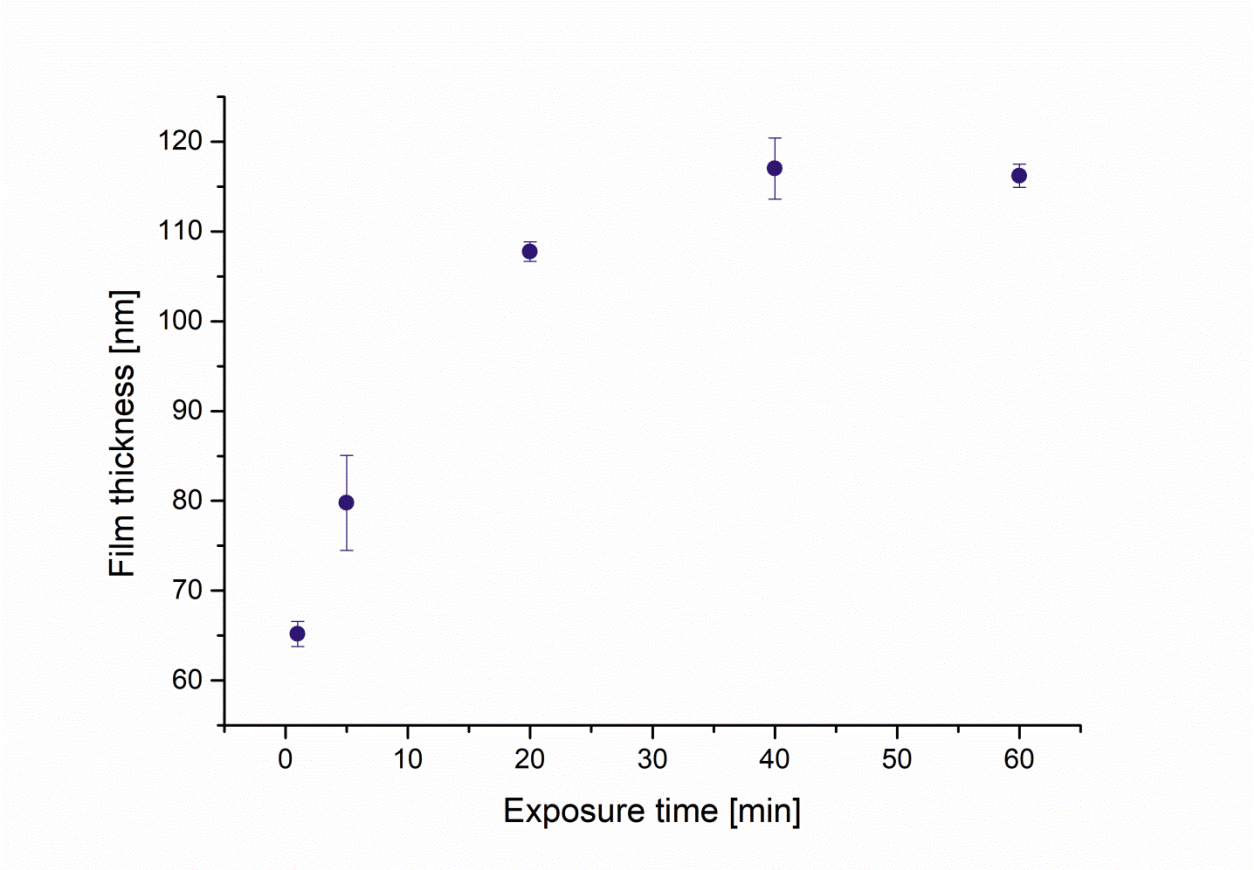

Figure 35: Thickness of the developed films illuminated with different exposure times.

Dark reaction time

According to Wolfberger et al. there is another process important for the desilylation after irradiation. The desilylation reaction does not end when the exposure to UV-light is stopped, but proceeds in absence of light for up to 24 h [80]. Photo-generated protons catalyze the reaction, even if there are no more protons produced. This process is referred to as *dark reaction* or *post exposure bake* and already known from cationic photo-polymerization reactions and traditional photolithography [38,81,82].

The dark reaction time was varied by extending the time between illumination and development from 30 min to 24 h. The film thickness of the regenerated films increases with dark reaction time (Figure 36).

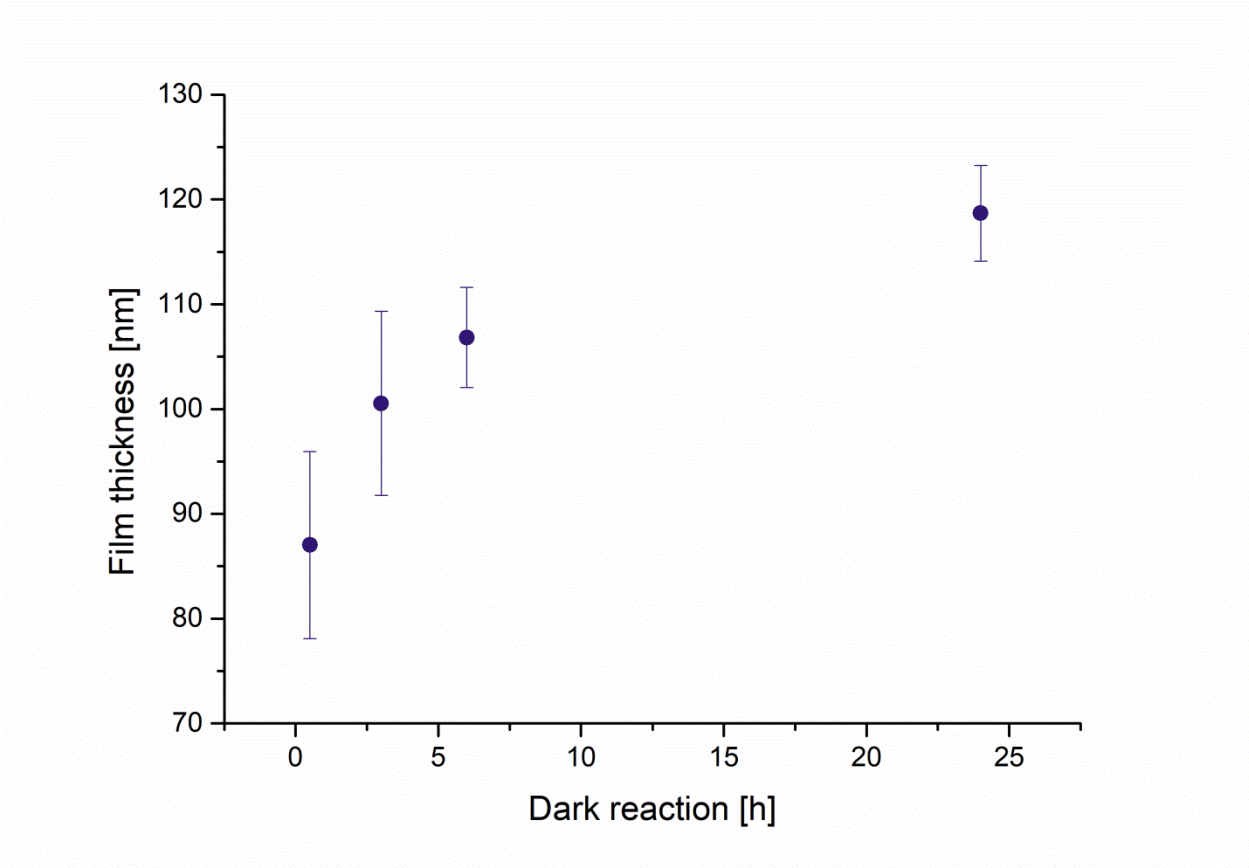

Figure 36: Thickness of the developed films after alteration of dark reaction times. 50 mg Si3S1/ml chloroform with 5 wt% PAG2; 20 min illumination with Heraeus lamp.

Evaluation of the optimal parameters:

From the previous experiments the optimal parameters can be combined to maintain the largest preserved film thickness (lowest lignin degradation?), and thereby the best regeneration efficiency, during the regeneration process of lignin from SiL. The lowest decrease in film thickness should be achieved by illumination with the Heraeus lamp for 40 minutes, using 5 % PAG2 as photo acid generator and allowing for dark reaction for at least 6 hours.

Surface properties during photo regeneration:

As a first, rough estimation by eye and a good estimation of regeneration after measurement the static water contact angle and the surface energy of the film can be used. Surface energies and contact angles of lignin and lignin derivatives can be found repeatedly in literature [3,8,35,36,83] and can therefore be used as reference values.

The water contact angle of SiL is high, with 87° (Figure 37). A high contact angle is achieved by very hydrophobic materials and can be increased by tuning the surface roughness, in the extreme case leading to almost perfect non-wettability and the so-called *lotus effect* [44]. According to Buono et al. a high contact angle is already achieved at a small percentages of silylation and conversion of 50 % should yield a contact angle of above 90° [8]. This finding correlates with a degree of silylation of 48% estimated by quantitative ^{1}H-NMR spectroscopy. After photo regeneration the contact angle is decreased and does not significantly change after development. However, the desired contact angle of pure lignin of about 50°, which can be obtained by regeneration in HCl vapour, was not achieved by illumination. This indicates an incomplete turnover in this regeneration process (50 mg/ml SiL in chloroform; 5 % PAG**2**; 20 min exposure time; 3 h dark reaction). However, solubility differences and patterning can be achieved.

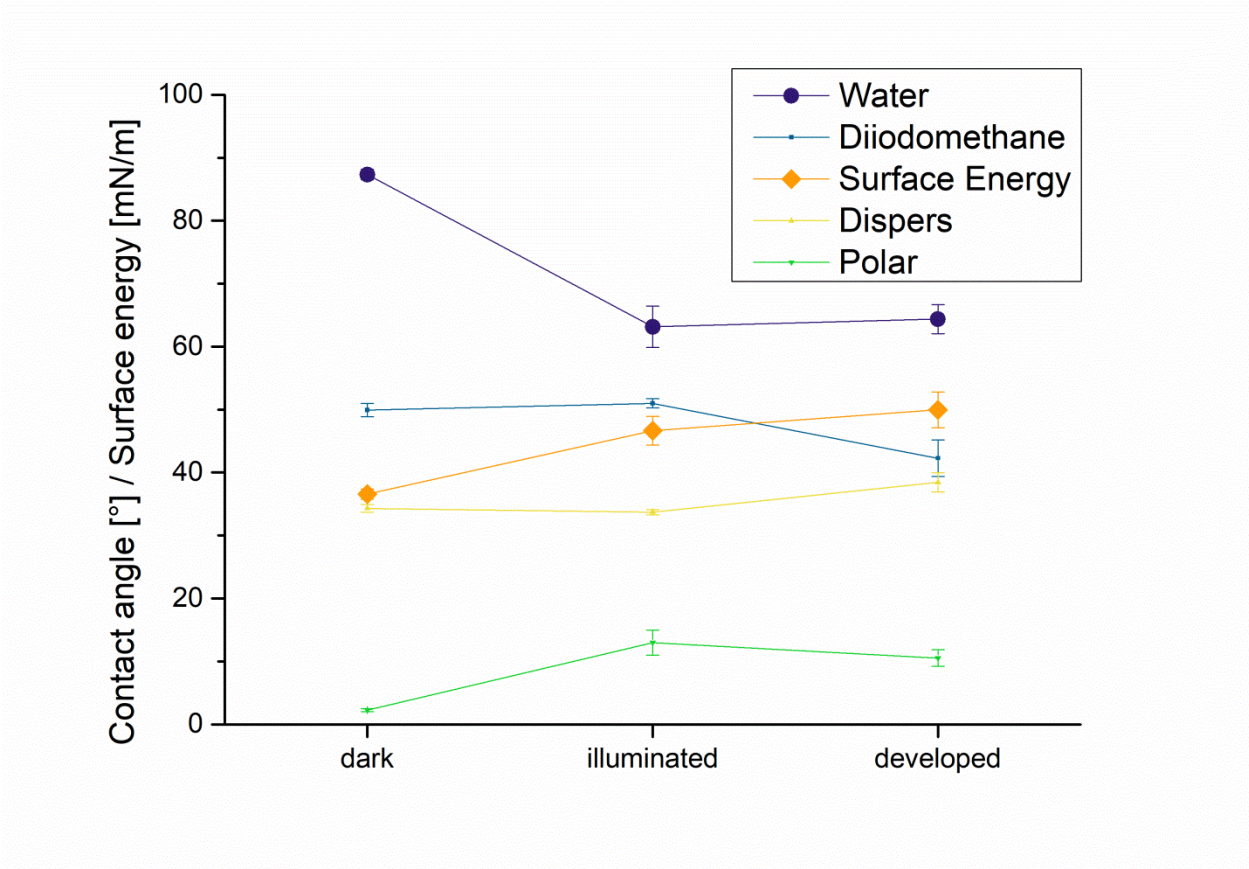

Figure 37: Contact angle and surface energy during illumination and development

The surface energy, determined by contact angle measurement of two liquids with known surface tension (water and diiodomethane), increased over the course of the regeneration experiment. However, the water contact angle remained constant after illumination, the contact angle of diiodomethane changed again after the developing step.

The photo regeneration process was also followed by AFM imaging. There was no distinct change in surface roughness and appearance during illumination, however, after washing the film showed an increased roughness (Figure 38). This could be the result of dissolution of the remaining non-recovered lignin (the thinning of the film was shown in profilometer measurements to be about 40 %) and a remaining of insoluble particles from the lignin sample. The phase image shows relatively high phase differences before illumination. This could be caused by the PAG, incorporated into the thin film. Legitimacy for this assumption is the almost constant phase found after illumination, which indicates a chemically homogeneous surface and the depletion of the photo acid generator. The phase after development is more diverse again, as the general surface roughness increases and steps contribute to the phase image.

The size of the aggregates did not change in this experiment, in contrast to the HCl-regeneration of Si2S1. The distinct sample properties and the way of regeneration may play a role in this phenomena, but more AFM experiments would be needed to investigate this behaviour in depth.

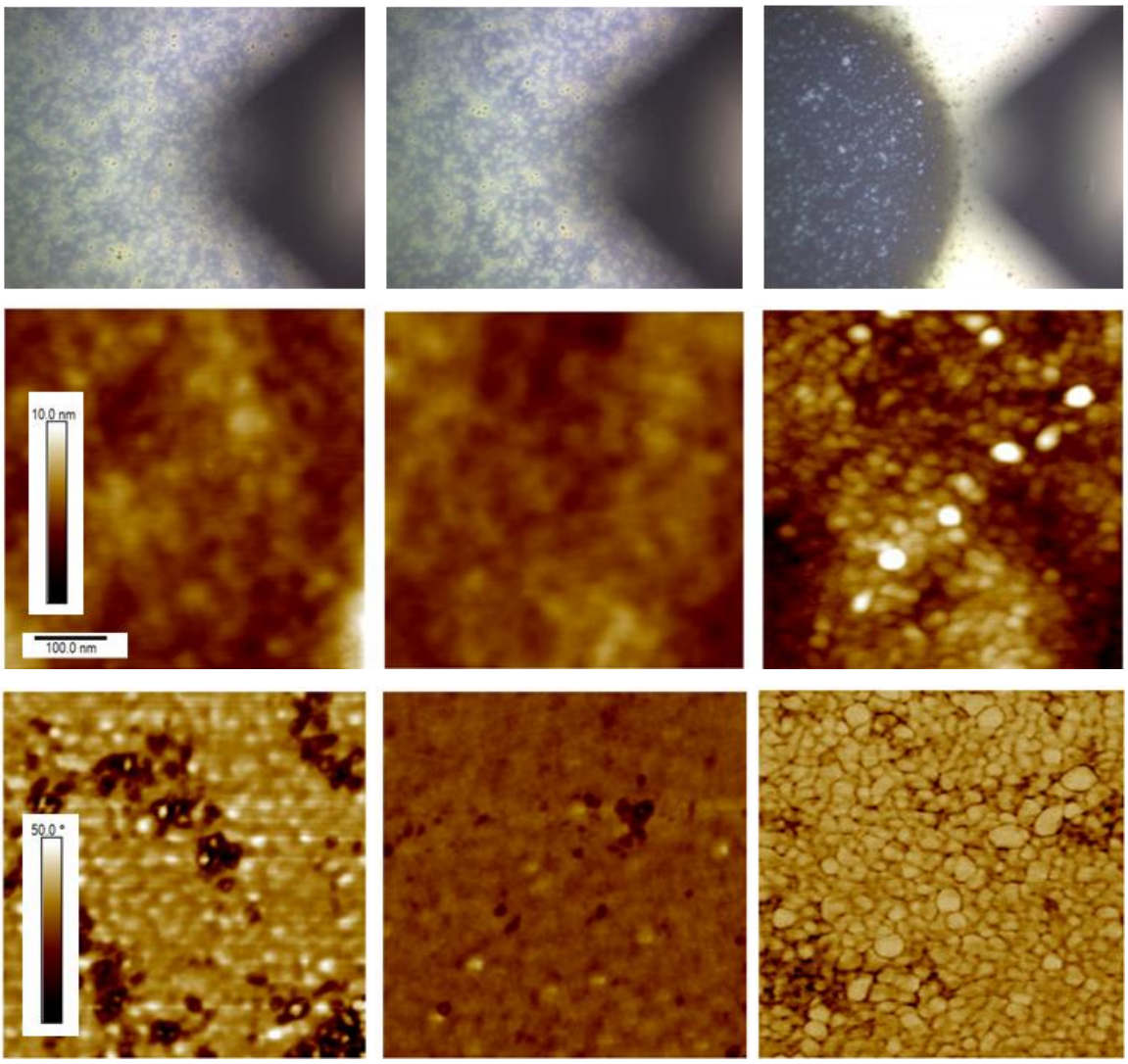

Figure 38: AFM images showing the change of the thin film surface (Si1S5; 50 mg/ml in chloroform) during the process of photo regeneration (before illumination (left); after illumination (middle); after washing with chloroform (right)). The upper row shows light microscopy images during the AFM imaging (with the cantilever out of focus), the second row shows the AFM height images with a data scale of 500 nm x 500 nm and a z-range of 10.0 nm and the third row shows the phase from AFM measurements (data scale of 500 nm x 500 nm).

4.4.3. Illumination without PAG – regeneration, cross-linking or degradation?

In addition to the regeneration of lignin with PAGs, also the regeneration of pure AcL and the possible cross linkage of lignin was tested. Therefore lignin and lignin acetate were subjected to UV irradiation. In a first try, when illuminating with a 6 W UV-lamp for 20 minutes on a gold substrate, no change could be seen in the ATR-IR spectra. However, when lignin (5mg/l) was dissolved in diluted ammonium hydroxide and exposed to UV light (Lightningcure LC4; Hamamtsu)

for 200 min a slow decrease in the characteristic bands, at 280 and 210 nm, in UV spectroscopy could be found (Figure 39). The peak at 280 nm corresponds to unconjugated phenolic hydroxyl groups and aromatic moieties, while the peak at 210 nm corresponds to portions of the unsaturated chains [84]. This decrease in absorption intensity is a sign for lignin degradation during the UV treatment, as it was prior reported in literature [84–87], however, at more intense irradiation conditions and mostly with photocatalysts added.

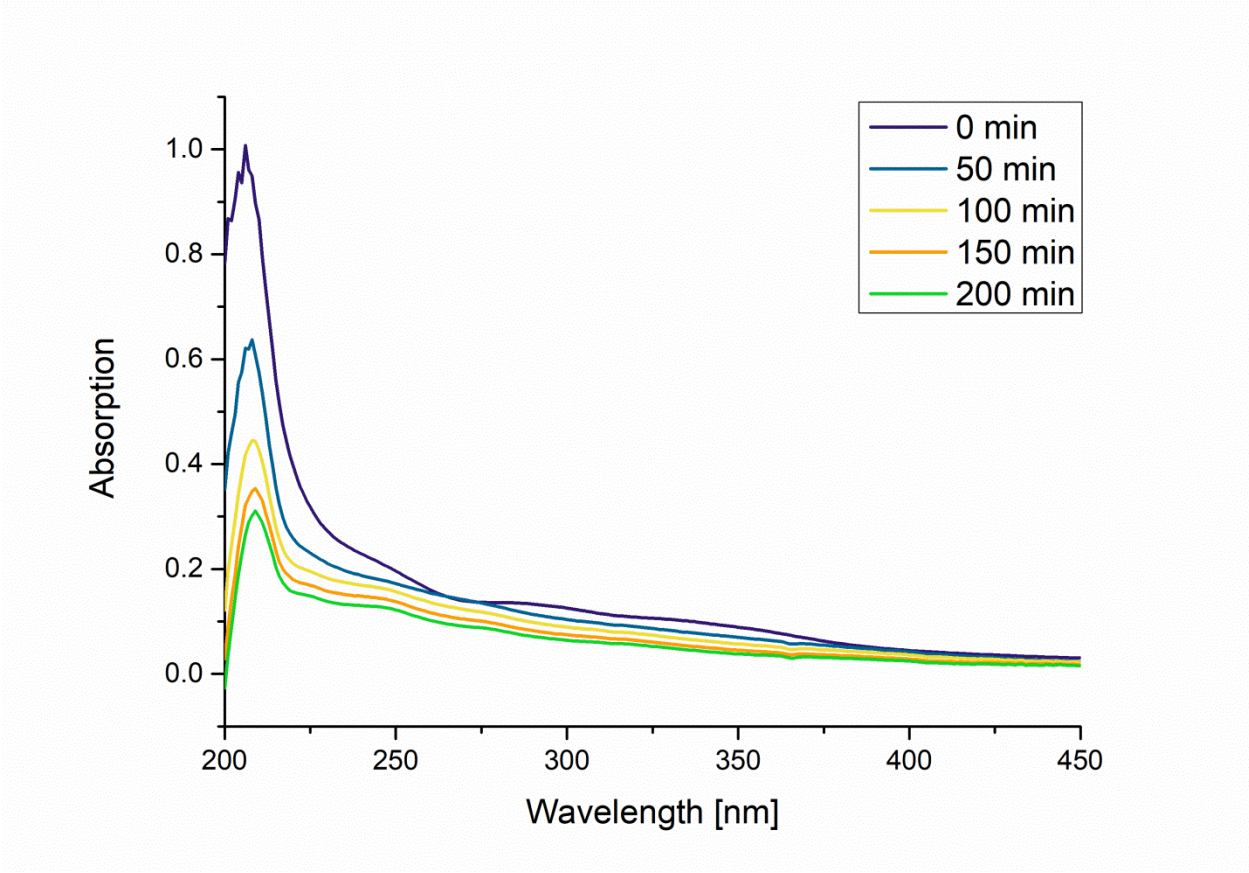

Figure 39: UV-VIS absorption spectra of lignin in ammonium hydroxide solution over time.

Figure 40: Illumination of lignin and lignin acetate on a gold slide for 20 minutes.

Further irradiation of thin films of lignin and lignin acetate coated from different solvents was investigated (Figure 40; Figure 41). ATR-IR spectra showed a distinct change in signals over time. Lignin (1 wt%) from ammonium hydroxide showed a relative increase in the ATR-IR band at 1160 cm^{-1}, while all other signals decreased over the time of 90 s. Lignin acetate solutions were coated from DMF, THF or chloroform, regenerated and exposed to UV light. The spectra of regenerated lignin were comparable showing the decrease of all bands, except the one at about 1770 cm^{-1}.

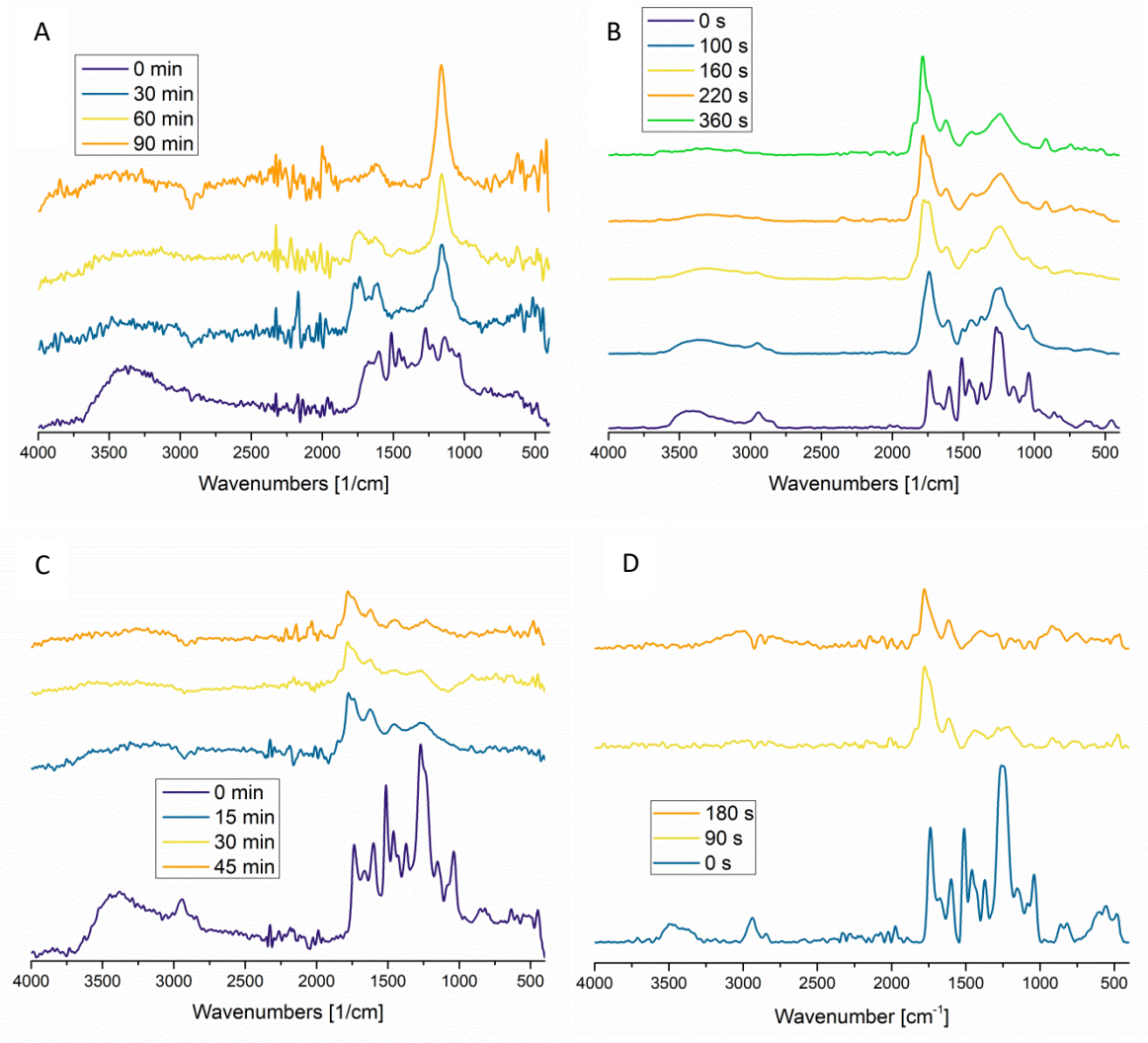

Figure 41: ATR-IR spectra of lignin during illumination for various time spans. Coated from (A) NH4OH, (B) THF (regenerated from AcL), (C) chloroform (regenerated from AcL) and (D) DMF (regenerated from AcL).

In a study on lignin degradation on $TiO_{2,}$ Tanaka et al. stated, that all bands assigned to aromatic rings disappeared as photo catalytic processes are oxidations via an OH radical, which degraded mainly aromatic moieties. The band at 1160 cm^{-1} might be due to SO_4^{2-} whereas the oneat 1770 cm^{-1} suggested the formation of carboxylates and/or aldehydes [85].

In contrast, various sources confirm the formation of breakdown products like benzaldehyde, benzoic acid, vanillin or syringaldehyde, during lignin degradation with photo catalysts [86–88]. Machado et al. also stated, that lignin degradation without catalyst is "*dominated by the electron transfer between the phenolate anion and ground state oxygen leading to the breakdown of the phenolic units*", while catalytic illumination results in a structural fragmentation of lignin [89].

According to Machado et al. the herein observed process might not function over the same pathway as catalytic degradation, but, nevertheless, seems to yield similar products. To confirm the statements given above, a more detailed molecular and elemental analysis (e.g. GC-MS) would be necessary.

Although there is a significant heating of the substrate while illumination, it seems unlikely that the structural change is caused by thermal degradation only. The temperatures are too low and thermal degradation should not result in a breakdown of aromatic structures [90]. However, the increased temperature on the sample surface might enhance the photo-induced degradation.

5. Conclusion

The patterning of lignin based thin films with UV-irradiation was successfully developed and the process parameters were optimized within the resources available.

Lignin derivative thin films with low roughness and good homogeneity could be produced. The film thickness was tuneable with the concentration of the spin coating solution ranging from 10 to 200 nm.

The structural changes for the solubility differences needed for successful patterning were obtained by introducing a hydrophobic substituent (-TMS) and cleaving off the silyl group with an acid upon irradiation. By adding a photoacid generator and producing an acid for regeneration of lignin in-situ, a good regeneration and solubility difference between regenerated lignin and the initial silylated lignin film was achieved.

Alterations in the surface structure of the lignin based thin films were monitored by atomic force microscopy, showing an increase of roughness and decrease of film thickness throughout the illumination experiment. This did, however, not affect the continuity of the residual film and should not be a problem in the use of this kind of system as a photoresist.

Besides the lignin films with PAG, pure lignin and lignin acetate were tested upon UV-irradiation and a different degradation behavior was observed. For a detailed description of the decomposition process and specification of the degradation products further experiments need to be carried out.

To conclude, the overall goal of this research project was achieved by finding a lignin based system exhibiting solubility differences upon irradiation. It is still a long way to go until biobased photoresists may compete with the much used synthetic polymers in terms of the patterning accuracy and resistance against etching chemicals, however, a first step towards the substitution of traditional photoresists has been taken.

6. References

[1] F. G. Calvo-Flores; J. A. Dobado; J. Isac-García; F. J. Martín-Martínez: Lignin and Lignans as Renewable Raw Materials: Chemistry, Technology and Applications, Wiley, **2015**.

[2] F.G. Calvo-Flores, J.A. Dobado, *ChemSusChem* 3 (**2010)** 1227–1235.

[3] S.M. Notley, M. Norgren, *Langmuir* 26 (**2010)** 5484–5490.

[4] M. Leisola, O. Pastinen, D.D. Axe, *BIO-Complexity* 2012 (**2012)**.

[5] T.-Q. Yuan, S.-N. Sun, F. Xu, R.-C. Sun, *Journal of agricultural and food chemistry* 59 (**2011)** 10604–10614.

[6] D. Fengel; G. Wegener: Wood: chemistry, ultrastructure, reactions, De Gruyter, **1983**.

[7] R. Whetten, R. Sederoff, *The Plant cell* 7 (**1995)** 1001–1013.

[8] P. Buono, A. Duval, P. Verge, L. Averous, Y. Habibi, *ACS Sustainable Chemistry & Engineering* 4 (**2016)** 5212–5222.

[9] D.R. Ratnaweera, D. Saha, S.V. Pingali, N. Labbé, A.K. Naskar, M. Dadmun, *RSC Advances* 5 (**2015)** 67258–67266.

[10] Y. Lu, Y.-C. Lu, H.-Q. Hu, F.-J. Xie, X.-Y. Wei, X. Fan, *Journal of Spectroscopy* 2017 (**2017)** 1–15.

[11] H. Semke: Charakterisierung, Funktionalisierung und Verarbeitung von Ligninen aus Dikotyledonen. Dissertation, Albert-Ludwigs-Universität Freiburg i. Br., **2001**.

[12] B. Ahvazi, É. Cloutier, O. Wojciechowicz, T.-D. Ngo, *ACS Sustainable Chemistry & Engineering* 4 (**2016)** 5090–5105.

[13] A. Vishtal, A. Kraslawski, *BioResources* 6 (**2011)** 3547–3568.

[14] F.S. Chakar, A.J. Ragauskas, *Industrial Crops and Products* 20 (**2004)** 131–141.

[15] B. Saake, R. Lehnen, in: Ullmann's Encyclopedia of Industrial Chemistry, Wiley-VCH Verlag GmbH & Co. KGaA, Weinheim, Germany, 2000, p. 45.

[16] J. Lora, in: M. Collins (Ed.), White Papers, University of Pittsburgh Press, 2012, pp. 225–241.

[17] D. Stewart, *Industrial Crops and Products* 27 (**2008)** 202–207.

[18] F.J. Lu, L.H. Chu, R.J. Gau, *Nutrition and cancer* 30 (**1998)** 31–38.

[19] V. Ugartondo, M. Mitjans, M.P. Vinardell, *Bioresource technology* 99 (**2008)** 6683–6687.

[20] Y. Yamamoto, H. Shirono, K. Kono, Y. Ohashi, *Bioscience, biotechnology, and biochemistry* 61 (**1997)** 1909–1912.

[21] H. Nägele, J. Pfitzer, E. Nägele, E.R. Inone, N. Eisenreich, W. Eckl, P. Eyerer, in: T.Q. Hu (Ed.), Chemical modification, properties, and usage of Lignin, 1st ed., Springer, New York, 2002, pp. 101–119.

[22] M. Norgren, H. Edlund, *Current Opinion in Colloid & Interface Science* 19 (**2014)** 409–416.

[23] M. Lersch: Creating value from wood - The Borregaard biorefinery, BIOREF-INTEG.

[24] E.B.d. Silva, M. Žabková, J.D. Araújo, C.A. Cateto, M.F. Barreiro, M.N. Belgacem, A.E. Rodrigues, *Chemical Engineering Research and Design* 87 (**2009)** 1276–1292.

[25] M. Žabková, E.B. da Silva, A.E. Rodrigues, *Journal of Membrane Science* 301 (**2007)** 221–237.

[26] I. C. Hoeger: Biocomponent films of cellulose and lignin and their biodegradation, Aalto University, **2011**.

[27] S.B. Lee, P. Luner, *TAPPI Journal* 55 (**1972)** 116–121.

[28] M. Micic, I. Benitez, M. Ruano, M. Mavers, M. Jeremic, K. Radotic, V. Moy, R.M. Leblanc, *Chemical Physics Letters* 347 (**2001)** 41–45.

[29] AdReNa Group UCL: Langmuir-Blodgett Trough Tutorial by Alaric, **2017**.
[30] D.S. Correa, E.S. Medeiros, J.E. Oliveira, L.G. Paterno, L.H.C. Mattoso, *Journal of Nanoscience and Nanotechnology* 14 (**2014)** 6509–6527.
[31] M. Norgren, S.M. Notley, A. Majtnerova, G. Gellerstedt, *Langmuir* 22 (**2006)** 1209–1214.
[32] Y. Chang, W.C. Wu, W.C. Chen, *Journal of The Electrochemical Society* 148 (**2001)** F77.
[33] T. Tammelin, M. Österberg, L.-S. Johansson, J. Laine, *Nordic Pulp and Paper Research Journal* 21 (**2006)** 444–450.
[34] C. Salas, O.J. Rojas, L.A. Lucia, M.A. Hubbe, J. Genzer, *ACS applied materials & interfaces* 5 (**2013)** 199–206.
[35] I.C. Hoeger, I. Filpponen, R. Martin-Sampedro, L.-S. Johansson, M. Osterberg, J. Laine, S. Kelley, O.J. Rojas, *Biomacromolecules* 13 (**2012)** 3228–3240.
[36] R. Martín-Sampedro, J.L. Rahikainen, L.-S. Johansson, K. Marjamaa, J. Laine, K. Kruus, O.J. Rojas, *Biomacromolecules* 14 (**2013)** 1231–1239.
[37] S. Strasser, K. Niegelhell, M. Kaschowitz, S. Markus, R. Kargl, K. Stana-Kleinschek, C. Slugovc, T. Mohan, S. Spirk, *Biomacromolecules* 17 (**2016)** 1083–1092.
[38] R.A. Lawson, A.P.G. Robinson, in: Materials and Processes for Next Generation Lithography, pp. 1–90.
[39] C. A. Mack: Fundamental Principles of Optical Lithography: The Science of Microfabrication, Wiley, **2008**.
[40] Y.-r. Jiang, J.-l. Li, H. Xu, *Chemical Research in Chinese Universities* 25 (**2009)** 870–875.
[41] Q. Lin, in: J.E. Mark (Ed.), Physical Properties of Polymers Handbook, Springer, New York, NY, 2007, pp. 965–979.
[42] M.M. Kohonen, *Langmuir* 22 (**2006)** 3148–3153.
[43] S.-J. Park, M.-K. Seo, in: Interface Science and Composites, pp. 147–252.
[44] L. Gao, T.J. McCarthy, *Langmuir* 25 (**2009)** 14105–14115.
[45] S.-J. Park, Seo, Min-Kang (Eds.): Interface Science and Composites: Volume 18, Elsevier, **2011**.
[46] D.K. Owens, R.C. Wendt, *Journal of Applied Polymer Science* 13 (**1969)** 1741–1747.
[47] Surface free energy, https://www.kruss-scientific.com/services/education-theory/glossary/surface-free-energy/, accessed 11.09.208.
[48] C. J. van Oss: Interfacial forces in aqueous media, Taylor & Francis Group, **2006**.
[49] A.B.D. Cassie, *Discussions of the Faraday Society* 3 (**1948)** 11.
[50] Biolin Scientific: Influence of surface roughness on contact angle and wettability: Theory note 7, http://biolinscientific.com/zafepress.php?url=%2Fpdf%2FAttension%2FTheory%20Notes%2FAT_TN_7_roughness.pdf, accessed 19 September 2018.
[51] L. Gao, T.J. McCarthy, *Langmuir* 23 (**2007)** 3762–3765.
[52] C.W. Extrand, *Langmuir* 19 (**2003)** 3793–3796.
[53] E.I. Evstigneev, *Russian Journal of Applied Chemistry* 84 (**2011)** 1040–1045.
[54] J. Sameni, S. Krigstin, M. Sain, *BioResources* 12 (**2016)**.
[55] W. Zhao, L.-P. Xiao, G. Song, R.-C. Sun, L. He, S. Singh, B.A. Simmons, G. Cheng, *Green Chemistry* 19 (**2017)** 3272–3281.
[56] B. Cathala, B. Saake, O. Faix, B. Monties, *Journal of Chromatography A* 1020 (**2003)** 229–239.
[57] J.M. Shaw, J.D. Gelorme, N.C. LaBianca, W.E. Conley, S.J. Holmes, *IBM Journal of Research and Development* 41 (**1997)** 81–94.

[58] A. Novembre, S. Liu, in: Nanolithography, pp. 194–286.
[59] A. Granata, D.S. Argyropoulos, *Journal of agricultural and food chemistry* 43 (**1995)** 1538–1544.
[60] F. Monteil-Rivera, L. Paquet, *Industrial Crops and Products* 65 (**2015)** 446–453.
[61] D.S. Argyropoulos, H.I. Bolker, C. Heitner, Y. Archipov, *Journal of Wood Chemistry and Technology* 13 (**1993)** 187–212.
[62] G.R. Fulmer, A.J.M. Miller, N.H. Sherden, H.E. Gottlieb, A. Nudelman, B.M. Stoltz, J.E. Bercaw, K.I. Goldberg, *Organometallics* 29 (**2010)** 2176–2179.
[63] F. Monteil-Rivera, L. Paquet, *Industrial Crops and Products* 65 (**2015)** 446–453.
[64] A. Ragauskas: Lignin Acetylation, http://biorefinery.utk.edu/technical_reviews/Lignin%20Acetylation.pdf, accessed 9 October 2018.
[65] L. Whalen: Microsoft Word - 05 IR chart, http://www.unm.edu/~orgchem/304L%20pages/05%20IR%20chart.pdf.
[66] B. C. Smith: Infrared spectral interpretation: A systematic approach, CRC Press, **1999**.
[67] T.E. Skrebets, K.G. Bogolitsyn, D.S. Kosyakov, S.A. Verbitskaya, *Russian Journal of Applied Chemistry* 77 (**2004)** 1536–1539.
[68] G. Motan, A. Puia, *Acta Chemica lasi* 22 (**2014)** 155–164.
[69] C.-L. Chen, D. Robert, *Methods in Enzymology* 161 (**1988)** 137-174.
[70] C. Nouvel, I. Ydens, P. Degée, P. Dubois, E. Dellacherie, J.-L. Six, *Polymer* 43 (**2002)** 1735–1743.
[71] R. Brežný, J. Schraml, M. Kvíčalová, J. Zelený, V. Chvalovský, *Holzforschung* 39 (**1985)** 297–303.
[72] F. Shirini, M.A. Zolfigol, K. Mohammadi, *Phosphorus, Sulfur, and Silicon and the Related Elements* 178 (**2003)** 1567–1570.
[73] R. Mörck, A. Reimann, K.P. Kringstad, *Holzforschung* (**1988)** 111–116.
[74] T.G. Rials, W.G. Glasser, *Polymer* 31 (**1990)** 1333–1338.
[75] D.G. Stavenga, *Materials Today: Proceedings* 1 (**2014)** 109–121.
[76] S. Bylin, T. Wells, Q. Sun, A. Ragauskas, H. Theliander, *BioResources* 9 (**2014)**.
[77] T. Maver, U. Maver, F. Mostegel, T. Griesser, S. Spirk, D.M. Smrke, K. Stana-Kleinschek, *Cellulose* 22 (**2015)** 749–761.
[78] K. Niegelhell, M. Süßenbacher, K. Jammernegg, T. Ganner, D. Schwendenwein, H. Schwab, F. Stelzer, H. Plank, S. Spirk, *Biomacromolecules* 17 (**2016)** 3743–3749.
[79] A. Wolfberger, R. Kargl, T. Griesser, S. Spirk, *Molecules* 19 (**2014)** 16266–16273.
[80] A. Wolfberger, A. Petritz, A. Fian, J. Herka, V. Schmidt, B. Stadlober, R. Kargl, S. Spirk, T. Griesser, *Cellulose* 22 (**2015)** 717–727.
[81] C. Decker, K. Moussa, *Journal of Polymer Science Part A: Polymer Chemistry* 28 (**1990)** 3429–3443.
[82] M. Kattan, E. Dargent, R.T. Olsson, *Journal of Thermal Analysis and Calorimetry* 76 (**2004)** 367–377.
[83] S.M. Notley, M. Norgren, *Holzforschung* 66 (**2012)** 615–622.
[84] C.A. Lekelefac, N. Busse, M. Herrenbauer, P. Czermak, *International Journal of Photoenergy* 2014 (**2015)** 1–18.
[85] K. Tanaka, R.C.R. Calanag, T. Hisanaga, *Journal of Molecular Catalysis A: Chemical* 138 (**1999)** 287–294.
[86] M. Tian, J. Wen, D. MacDonald, R.M. Asmussen, A. Chen, *Electrochemistry Communications* 12 (**2010)** 527–530.
[87] M. Ksibi, *Journal of Photochemistry and Photobiology A: Chemistry* 154 (**2003)** 211–218.
[88] M. Azadfallah, S.A. Mirshokraei, A.J. Latibari, *Molecules* 13 (**2008)** 3129–3139.

[89] A.E.H. Machado, A.M. Furuyama, S.Z. Falone, R. Ruggiero, D.d.S. Perez, A. Castellan, *Chemosphere* 40 (**2000)** 115–124.

[90] I.A.K. Reddy, H.R. Ghatak, *Journal of Thermal Analysis and Calorimetry* 132 (**2018)** 407–423.

7. Appendix

7.1. Sample Preparation for Zellstoff Pöls Lignin (S3-S5)

Lignin Pöls unwashedj (S3)

The lignin filter cake from the pilot plant (80 l) at the paper plant from Zellstoff Pöls AG was precipitated until a pH of 9-9.5 at room temperature. The filter cake had 69 % of solid content (DS) and 24 % ash in the solid. The sample was taken in November 2017 and was stored at -18°C and later at room temperature.

Lignin water washed (S4)

The lignin filter cake from the pilot plant (80 l) at the paper plant from Zellstoff Pöls AG was mixed with five times the volume of destilled water at room temperature. The mixture was stirred for 5 minutes, filtered and the procedure was repeated. There was a loss in mass of the filter cake, as parts of the lignin were soluble. The resulting filter cake was dired in the oven at 60°C. The DS is 90-100 % and the ash in the dried sample is about 8 %.

Lignin acid washed (S5)

The lignin filter cake from the pilot plant (80 l) at the paper plant from Zellstoff Pöls AG was mixed with five times the volume of sulfuric acid (200 g H2SO4 in 1 l water at 60°C), stirred for 5 minutes and filtered. The procedure was repeated with water at pH 1. The filter cake was dried in the oven at 60°C and stored in an exsiccator. The DS is 90-100 % and the ash in the dried sample is about 0.5-1.0 %.